NASA/TM—2006-214477

Development and Testing of a Radial Halbach Magnetic Bearing

Dennis J. Eichenberg, Christopher A. Gallo, and William K. Thompson
Glenn Research Center, Cleveland, Ohio

December 2006

NASA STI Program . . . in Profile

Since its founding, NASA has been dedicated to the advancement of aeronautics and space science. The NASA Scientific and Technical Information (STI) program plays a key part in helping NASA maintain this important role.

The NASA STI Program operates under the auspices of the Agency Chief Information Officer. It collects, organizes, provides for archiving, and disseminates NASA's STI. The NASA STI program provides access to the NASA Aeronautics and Space Database and its public interface, the NASA Technical Reports Server, thus providing one of the largest collections of aeronautical and space science STI in the world. Results are published in both non-NASA channels and by NASA in the NASA STI Report Series, which includes the following report types:

- TECHNICAL PUBLICATION. Reports of completed research or a major significant phase of research that present the results of NASA programs and include extensive data or theoretical analysis. Includes compilations of significant scientific and technical data and information deemed to be of continuing reference value. NASA counterpart of peer-reviewed formal professional papers but has less stringent limitations on manuscript length and extent of graphic presentations.

- TECHNICAL MEMORANDUM. Scientific and technical findings that are preliminary or of specialized interest, e.g., quick release reports, working papers, and bibliographies that contain minimal annotation. Does not contain extensive analysis.

- CONTRACTOR REPORT. Scientific and technical findings by NASA-sponsored contractors and grantees.

- CONFERENCE PUBLICATION. Collected papers from scientific and technical conferences, symposia, seminars, or other meetings sponsored or cosponsored by NASA.

- SPECIAL PUBLICATION. Scientific, technical, or historical information from NASA programs, projects, and missions, often concerned with subjects having substantial public interest.

- TECHNICAL TRANSLATION. English-language translations of foreign scientific and technical material pertinent to NASA's mission.

Specialized services also include creating custom thesauri, building customized databases, organizing and publishing research results.

For more information about the NASA STI program, see the following:

- Access the NASA STI program home page at *http://www.sti.nasa.gov*

- E-mail your question via the Internet to *help@sti.nasa.gov*

- Fax your question to the NASA STI Help Desk at 301–621–0134

- Telephone the NASA STI Help Desk at 301–621–0390

- Write to:
  NASA STI Help Desk
  NASA Center for AeroSpace Information
  7115 Standard Drive
  Hanover, MD 21076–1320

NASA/TM—2006-214477

Development and Testing of a Radial Halbach Magnetic Bearing

Dennis J. Eichenberg, Christopher A. Gallo, and William K. Thompson
Glenn Research Center, Cleveland, Ohio

National Aeronautics and
Space Administration

Glenn Research Center
Cleveland, Ohio 44135

December 2006

Acknowledgments

This work was funded by NASA's Fundamental Aeronautics Program under project manager James F. Walker. The authors would like to thank Dawn C. Emerson (NASA Glenn Research Center) for assistance with the development of the analytical models, and Mark Christini (Ansoft Corp., Pittsburgh, PA) for assistance with the finite element analyses.

This work was sponsored by the Fundamental Aeronautics Program at the NASA Glenn Research Center.

Level of Review: This material has been technically reviewed by technical management.

Available from

NASA Center for Aerospace Information
7115 Standard Drive
Hanover, MD 21076–1320

National Technical Information Service
5285 Port Royal Road
Springfield, VA 22161

Available electronically at http://gltrs.grc.nasa.gov

Development and Testing of a Radial Halbach Magnetic Bearing

Dennis J. Eichenberg, Christopher A. Gallo, and William K. Thompson
National Aeronautics and Space Administration
Glenn Research Center
Cleveland, Ohio 44135

Summary

The NASA John H. Glenn Research Center has developed and tested a revolutionary Radial Halbach Magnetic Bearing. The objective of this work is to develop a viable non-contact magnetic bearing utilizing Halbach arrays for all-electric flight, and many other applications. This concept will help reduce harmful emissions, reduce the Nation's dependence on fossil fuels and mitigate many of the concerns and limitations encountered in conventional axial bearings such as bearing wear, leaks, seals and friction loss. The Radial Halbach Magnetic Bearing is inherently stable and requires no active feedback control system or superconductivity as required in many magnetic bearing designs. The Radial Halbach Magnetic Bearing is useful for very high speed applications where conventional bearings cannot be used including turbines, instrumentation, and medical applications. In addition, this technology has potential application in ultra-efficient motors, computer memory systems, manufacturing equipment and space power systems such as flywheels.

The Radial Halbach Magnetic Bearing employs many advanced technologies. The innovative physical layout consists of a rotor and a stator. The rotor is contained within a static shell assembly or stator. Magnetic fields suspend and support the rotor assembly within the stator. Advanced technologies developed for particle accelerators, and currently under development for maglev trains and rocket launchers, served as the basis for this application.

A small scale experimental hardware system was successfully designed and developed to validate the basic principles described, and the theoretical work that was performed. The report concludes that the implementation of Radial Halbach Magnetic Bearings can provide significant improvements in rotational system performance and reliability.

Introduction

The NASA Glenn Research Center has a wealth of experience in Halbach bearing technology through the Fundamental Aeronautics Program. The goals of the program include improving aircraft efficiency, reliability, and safety. The Radial Halbach Magnetic Bearing discussed in this report was developed under the Fundamental Aeronautics Program.

The electromagnetic concept of the Radial Halbach Magnetic Bearing uses permanent magnet elements attached to the circumference of the rotor, and wire coils placed in the stator shell. The permanent magnets are arranged in a "Halbach" configuration which results in the production of a sinusoidally varying, periodic magnetic field in the vicinity of the stator coils. This magnetic array configuration was pioneered by Klaus Halbach for use in particle accelerators (ref. 1). When the rotor is set in motion, the time varying magnetic fields interact with the passive coils in the stator assembly to produce repulsive forces between the stator and the rotor providing magnetic suspension. The system is inherently stable once the rotor reaches critical speed, and thus requires no active feedback control or superconductivity as seen in many traditional implementations of magnetic suspension.

Theoretical derivations have been developed to predict the levitation forces generated by a circular Halbach array and coil assembly. Finite element analyses were then performed to validate the theoretical derivations. Finally, experimental hardware was successfully designed and developed which served to validate the basic principles described and the theoretical work that was performed.

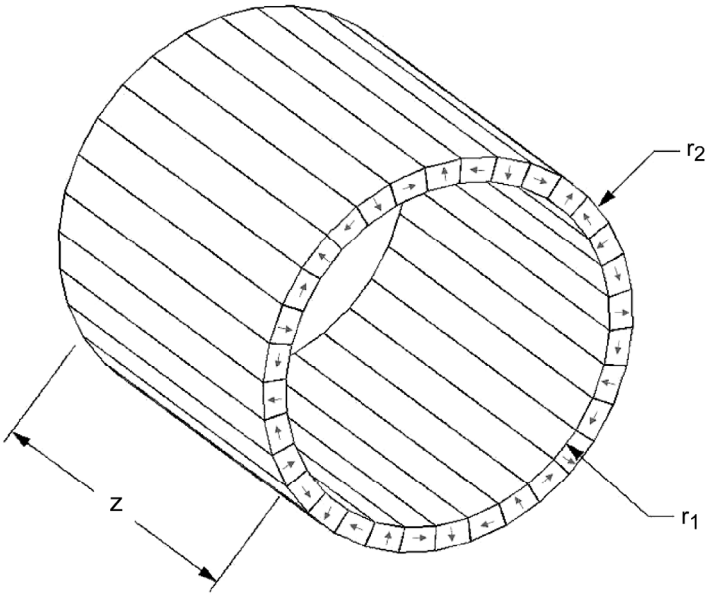

Figure 1.—The radial Halbach array for N_m = 32 magnets. Arrows indicate the direction of magnetization for each individual magnet. This particular arrangement will concentrate the B field outside the ring and cancel it inside the ring.

Electromagnetic Analysis

Magnetostatic Field

Figure 1 shows a typical arrangement of N_m magnets comprising an external field axial Halbach array. In this case there are N_m = 32 sector-shaped permanent magnets with an inner radius r_1, an outer radius r_2, an axial length Z, and four magnets per Halbach wavelength in the azimuthal (i.e., ϕ) direction. The number of pole pairs is therefore $p = N_m/4$. Each magnet has an index, s = [0, 1, … N_m–1], and a magnetization $M = \pm 4\pi B_r/\mu_o$, whose direction is indicated by the arrows. B_r is the remanent magnetization of the permanent magnet material.

Post determined previously (ref. 2) that the radial component of the field, B_ρ, at a radial distance $r > r_2$ is

$$B_\rho(r) = B_o \left(\frac{r_2}{r}\right)^{p+1} \cos p\phi \tag{1}$$

and the azimuthal component, B_ϕ, is

$$B_\phi(r) = B_o \left(\frac{r_2}{r}\right)^{p+1} \sin p\phi \tag{2}$$

where

$$B_o = B_r \frac{p}{p+1}\left[1 - \left(\frac{r_1}{r_2}\right)^{p+1}\right] C_n \tag{3}$$

and

$$C_n = \cos^p\left(\frac{\pi}{4p}\right)\left[\frac{\sin(\pi/4)}{\pi/4}\right] \tag{4}$$

At sufficiently large values of gap distance, $g = r - r_2$, the field components exhibit sinusoidal behavior versus azimuthal position, ϕ. While additional harmonics in the field components arise at gap values that are small compared to the magnet thickness, a large enough stator winding smoothes out these harmonics in the flux calculations. All three field components also exhibit an inverse power law behavior with increasing gap distance, *g*. Writing equations (1) and (2) as a function of gap distance gives the radial field component as

$$B_\rho(g) = B_o\left(\frac{r_2}{r_2 + g}\right)^{p+1} \cos p\phi \tag{5}$$

and the azimuthal component as

$$B_\phi(g) = B_o\left(\frac{r_2}{r_2 + g}\right)^{p+1} \sin p\phi \tag{6}$$

Flux, EMF, current and force calculations for an r–z stator pole piece

Consider the stator pole piece shown in figure 2 which is window frame shaped and wound radially, i.e., the plane of the center of the stator winding lies in the *r-z* plane at azimuthal location $\phi = 0$. The normal vector of this plane coincides with the $\hat{\phi}$ direction. The winding consists of N_t turns, the width of

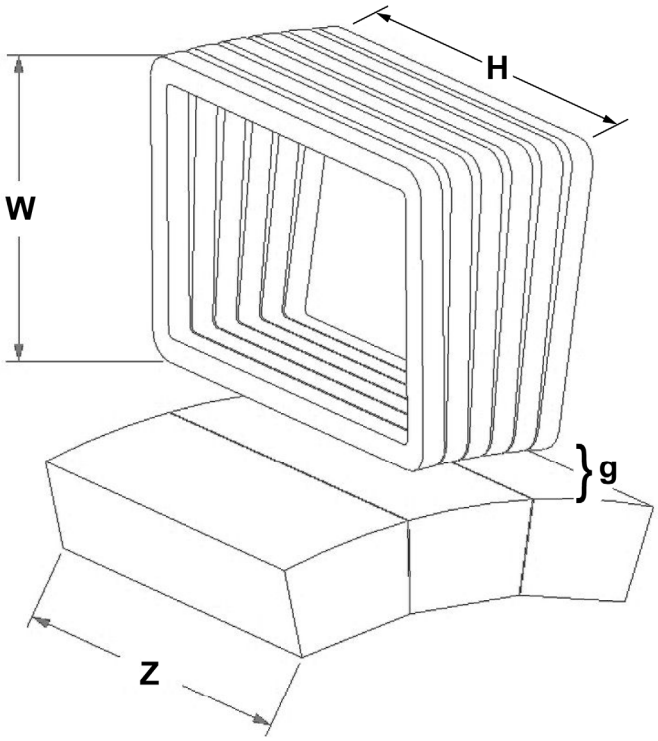

Figure 2.—A 6-turn r-z stator winding viewed from one end of the magnet array. The azimuthal span of the winding matches the width of one magnet. H and W refer to the winding height and width, respectively. A gap, g, exists between the center of the nearby conductors of the winding and the magnet surface.

the winding in the radial direction is *W,* and the height of the winding in the axial direction is *H*. *H* is chosen to be approximately the axial magnet length, *Z*. The size of *W* is critical. *W* must be large enough to minimize the Lorentz force interaction between the returning current and the B_ϕ field, while minimizing the stator resistance, which tends to reduce the lifting force and increase the drag force and power dissipation. The number of stator turns, N_t, is chosen to make the angular span of the winding approximately equal to one magnet width. A gap, *g*, exists between the outer radial surface of the magnets and the center of the nearby conductors of the winding. The radial location of the inner leg of the winding is $R_1 = r_2 + g$ and the outer leg is located at $R_2 = r_2 + g + W$.

To compute the stator flux, integrate the field component normal to the winding plane over the surface enclosed by the stator winding. For an *r-z* winding the flux as a function of angular position is given by Faraday's Law as

$$\Phi_{r-z}(\phi) = N_t w \int_S B_\phi(\vec{r}) \bullet dS = N_t w Z \int_{R_1}^{R_2} B_\phi(r)\, dr = \frac{B_r N_t w Z r_2}{p}\left[\left(\frac{r_2}{r_2+g}\right)^p - \left(\frac{r_2}{r_2+g+W}\right)^p\right]\sin(p\phi) \tag{7}$$

The winding factor, $w = w_1 w_2$, accounts for the spatial variance of the *B* field over the azimuthal span and the radial depth of the winding, respectively. The first winding factor component, w_1, is the intra-layer average of the winding. It is computed as the average over all winding turns when the peak of a cosine function coincides with the center of the winding. There are $N_t = N_{tz} N_{t\phi}$ total turns. If there are $N_{t\phi}$ turns in each layer, then w_1 is given by

$$w_1 = \begin{cases} \dfrac{2}{N_{t\phi}} \displaystyle\sum_{n=0}^{\frac{N_{t\phi}}{2}-1} \cos\left(\dfrac{\left(n+\frac{1}{2}\right)(d+\varepsilon)p}{r_2+g}\right) & \text{for } N_{t\phi} \text{ even} \\ \dfrac{1}{N_{t\phi}}\left[1 + 2\displaystyle\sum_{n=1}^{\frac{N_{t\phi}}{2}-1} \cos\left(\dfrac{n(d+\varepsilon)p}{r_2+g}\right)\right] & \text{for } N_{t\phi} \text{ odd} \end{cases} \tag{8}$$

The second winding factor, w_2 is the inter-layer average of the winding. It is computed as the average over all layers of the radial decay factor when the nearest layer is normalized to unity. If there are N_{tz} layers, then w_2 is given by

$$w_2 = \frac{1}{N_{tz}} \sum_{n=0}^{N_{tz}-1} \left(\frac{r_2}{r_2 + g + n(d+\varepsilon)}\right)^{p+1} \tag{9}$$

In these expressions *d* is the diameter of the conductor comprising the stator winding, ε is the average distance between the individual turns. If the winding spans approximately the same angle as one magnet and $N_{tz} = 1$ layer, then $w \approx 0.9$ and this factor may be taken outside the integral. For other winding geometries the winding factor may be computed as a spatial average over the axial span and axial depth of the winding and then taken outside the integral.

Assume that the array now rotates at a constant angular velocity $\omega = 2\pi \times rpm/60$, where *rpm* is the rotational speed expressed in revolutions per minute. The initial rotary position of the array relative to the static Halbach array case is $\phi_t = 0$. Therefore

$$\phi = -\omega t \tag{10}$$

and the flux therefore becomes a sinusoidal function of time given by

$$\Phi_{r-z}(t) = -\frac{B_r N_t w H r_2}{p}\left[\left(\frac{r_2}{r_2+g}\right)^p - \left(\frac{r_2}{r_2+g+W}\right)^p\right]\sin(p\omega t) \tag{11}$$

Since there are p Halbach arrays in the disk, the electrical frequency becomes $p\omega = N_m\omega/4$. Using equation (11) and Faraday's law, the open circuit voltage becomes

$$V_{oc}(t) = -\frac{d\Phi_{r-z}(t)}{dt} = B_o N_t w\ H\ \omega\ r_2\left[\left(\frac{r_2}{r_2+g}\right)^p - \left(\frac{r_2}{r_2+g+W}\right)^p\right]\cos(p\omega t) \tag{12}$$

Dividing by the complex impedance of the stator winding, including any external series components, and rearranging terms gives

$$I(t) = \frac{B_o N_t w\ H\ r_2}{pL}\left[\left(\frac{r_2}{r_2+g}\right)^p - \left(\frac{r_2}{r_2+g+W}\right)^p\right]\left[\frac{1}{1+\left(\frac{R}{p\omega L}\right)^2}\right]\cdot\left[\sin(p\omega t)+\left(\frac{R}{p\omega L}\right)\cdot\cos(p\omega t)\right] \tag{13}$$

Here R and L represent the total resistance and inductance, respectively, of the stator winding circuit. These impedances represent the lumped values of the stator self-resistance (R_s), self-inductance (L_s), any mutual inductances between windings, and any external passive components. Typically, an external coil with resistance R_c and inductance L_c may be added in series with the stator winding. The purpose of the external coil is to optimize the phase shift of the voltage and current, which maximizes axial force production (lift) while minimizing transverse plane force production (drag). For the arrangement under consideration, it is necessary that the phase angle between the voltage and current be as close to $\pi/2$ as practical so that the current is flowing axially downward (i.e., $-z$) when a $-\phi$ polarized magnet is passing over the stator so that lift force ($+r$) may be produced. Thus the total resistance is $R = R_s + R_c$ and the total inductance is $L = L_s + L_c$.

The current may be decomposed into its imaginary (lift-producing) and real (drag-producing) components. One may note, by comparing equations (13) with (5) and (6) that the lift current is in phase with B_ϕ field component and the drag current is in phase with the B_r component. The Lorentz force on the stator winding centered radially at gap distance g from the magnets is derived from $dF = Id\ell \times B$ as

$$F_{Lift,avg} = \left[\frac{B_o{}^2 N_t{}^2 H^2 w^2 r_2}{2pL}\right]\left(\frac{r_2}{r_2+g}\right)^p\left[\left(\frac{r_2}{r_2+g}\right)^p - \left(\frac{r_2}{r_2+g+W}\right)^p\right]\cdot\left[\frac{1}{1+\left(\frac{R}{p\omega L}\right)^2}\right] \tag{14}$$

$$F_{Drag,avg} = \left[\frac{B_o{}^2 N_t{}^2 H^2 w^2 r_2}{2pL}\right]\left(\frac{r_2}{r_2+g}\right)^p\left[\left(\frac{r_2}{r_2+g}\right)^p - \left(\frac{r_2}{r_2+g+W}\right)^p\right]\cdot\left[\frac{\frac{R}{p\omega L}}{1+\left(\frac{R}{p\omega L}\right)^2}\right] \tag{15}$$

The factor of ½ arises from the multiplication of two sinusoids of the same frequency. From the previous expressions, it should be noted that both the lift and drag forces vary with the square of the magnetic field strength at the magnet surface ($B_o{}^2$), the square of the number of stator turns ($N_t{}^2$) and the square of the winding factor (w^2). Equation (3) gives B_o as a linear function of the strength of the magnets (B_r) and as a nonlinear function of the ratio of the magnet inner and out radii (i.e., r_1/r_2). Force production falls off with increasing gap distance g as a power law dependence on the ratio of the outer magnet

radius (r_2) to the radial position of the winding (r_2+g). Scaling the machine diameter (i.e., varying r_2) is more complex due to the nonlinear explicit dependence of force production on this parameter, as well as the non-linear implicit dependence of R and L on this parameter.

The stator winding circuit resistances and inductances determine both the saturation value of the lift force and the rotational speed at which saturation is achieved. The drag force outpaces the lift force at low rotational speeds but reaches a maximum value at a critical speed given by (ref. 2)

$$\omega_c = \frac{1}{p}\frac{R}{L} \tag{16}$$

and then rolls off toward zero at high speeds. The expressions for lift and drag force are per stator pole, so the net forces must be summed as vectors over all poles.

Test Objectives

The objective of testing the Radial Halbach Magnetic Bearing is to validate the derived theoretical analyses and associated finite element analyses. This validation provides confidence in using the derived and numerical analyses for developing and optimizing conceptual Radial Halbach Magnetic Bearing designs.

Testing of the Radial Halbach Magnetic Bearing was performed at the NASA Glenn Research Center. To ascertain the effectiveness of the bearing, performance data are of particular interest. Force, voltage, current, and temperature were monitored at various rotor operating speeds.

Test Hardware Description

Two Radial Halbach Magnetic Bearing Test Models were developed. One test model includes a 4 in. long by 4 in. nominal diameter rotor as shown in figure 3 and the other includes a 1 in. long by 1 in. nominal diameter rotor as shown in figure 4. The Radial Halbach Magnetic Bearing Test Model block diagram is shown in figure 5. The Test Model components are identified in figure 6. This test hardware includes the support structure, force measurement scale and positioning system, and drive system components.

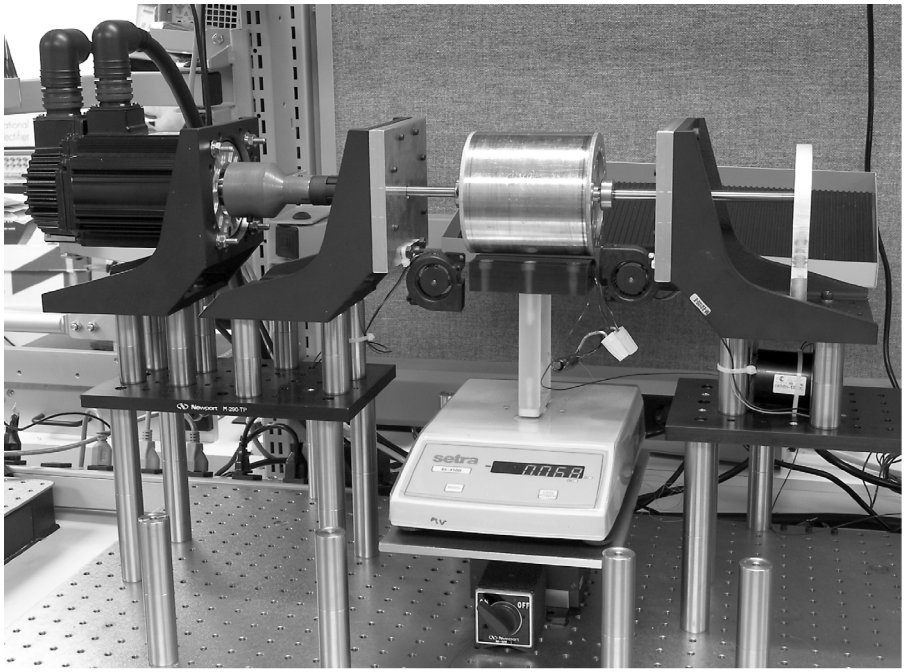

Figure 3.—Four inch radial Halbach magnetic bearing test model.

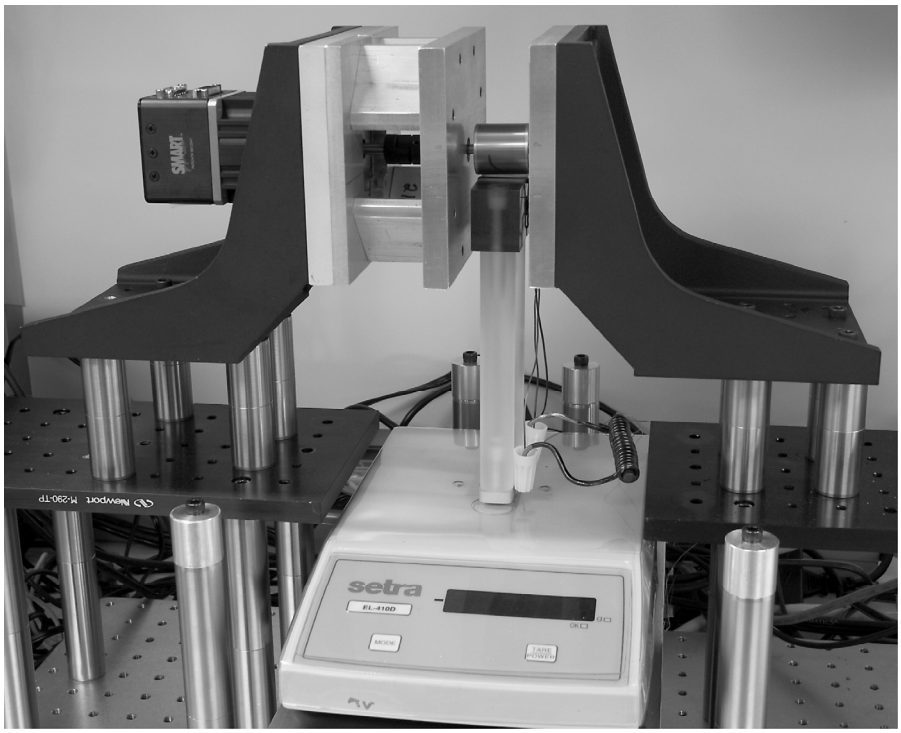

Figure 4.—One inch radial Halbach magnetic bearing test model.

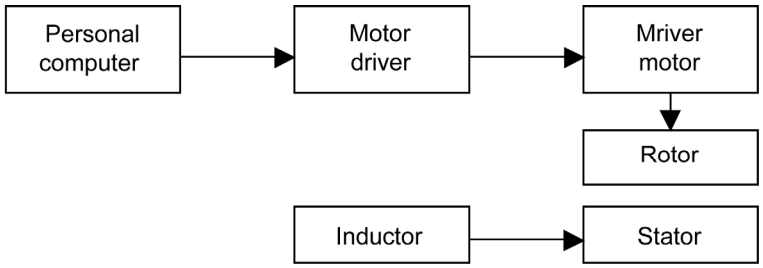

Figure 5.—Radial Halbach magnetic bearing test model block diagram.

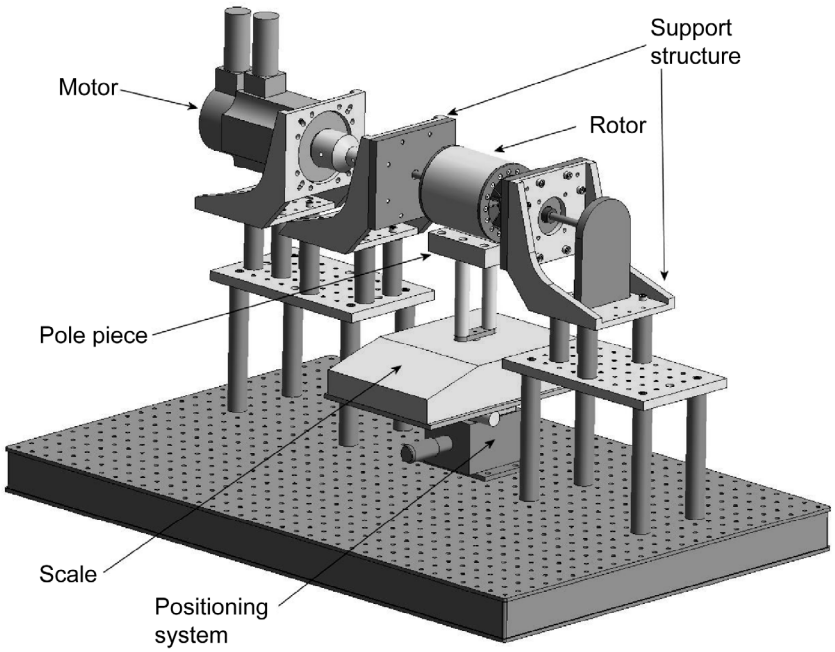

Figure 6.—Radial Halbach magnetic bearing test model components.

The support structure consists of precision structural components that are securely fastened to a heavy optics plate. The motor and the drive shaft bearing blocks are connected to right angle brackets that are connected to the optics plate via posts. This subsystem supports and aligns the drive system with respect to the scale and positioning system that is placed on the optics plate. A safety shield is fastened to the optics plate to protect personnel from the rotating components of the drive system and rotor.

The drive system for the 4 in. test model consists of a variable speed computer controlled motor that is connected to a 3/8 in. diameter drive shaft through a flexible coupling to allow for misalignment. The drive shaft is supported by two roller bearings secured in the bearing blocks. The rotor assembly is clamped to the drive shaft between the two bearings and is driven by the motor to maintain precise operating speed. The 1 in. test model drive system has a similar arrangement except that the motor used to drive the rotor is connected to a 5 mm shaft. The 1 in. rotor assembly is pinned to the drive shaft and is also located between the two bearings.

The 4 in. rotor assembly, as shown in figures 7 and 8, has an overall diameter of 4.15 in. and an overall length (not counting the two half in. clamping rings) of 4.31 in. The outer layer of the rotor consists of a 0.070 in. thick 300 series stainless steel shroud that is used to contain the 128 Neodymium Iron Boron B55 magnets. The magnets are 1/4 in. thick by 1 in. long segments. There are 32 segments around the circumference oriented in a Halbach array to make a ring and there are 4 rings total along the length of the rotor. The outside diameter of the magnet ring is 4 in. and each magnet segment occupies 11.25° of the assembled magnet ring. The magnets have a light press fit between the shroud and the hub that was wire electrical discharged machined from 6061-T6 aluminum. The hub has 32 flat surfaces machined around the circumference to support the back side of the magnets which is flat. The magnets are held in the rotor axially by two aluminum endplates which are fastened to the hub with non-magnetic stainless steel screws. Total weight of the assembled rotor is 2.8 kg (6.2 lb).

The 1 in. rotor assembly has an overall diameter of 1.06 in. and an overall length of 1.14 in. The outer layer of the rotor consists of a 0.030 in. thick 300 series stainless steel shroud that is used to contain the 16 Neodymium Iron Boron B55 magnets. The magnets are 1/8 in. thick by 1 in. long segments. There are 16 segments around the circumference oriented in a Halbach array to make a ring. The outside diameter of the magnet ring is 1 in. and each magnet segment occupies 22.5° of the assembled magnet ring. The magnets have a light press fit between the shroud and the hub that was wire electrical discharged machined from 6061-T6 aluminum. The hub has 16 flat surfaces machined around the circumference to support the back side of the magnets which is flat. The magnets are held in the rotor axially by two

aluminum endplates fastened to the hub with non-magnetic stainless steel screws. Total weight of the assembled rotor is 94 g (0.21 lb).

Figure 7.—Radial Halbach magnetic bearing test model rotor.

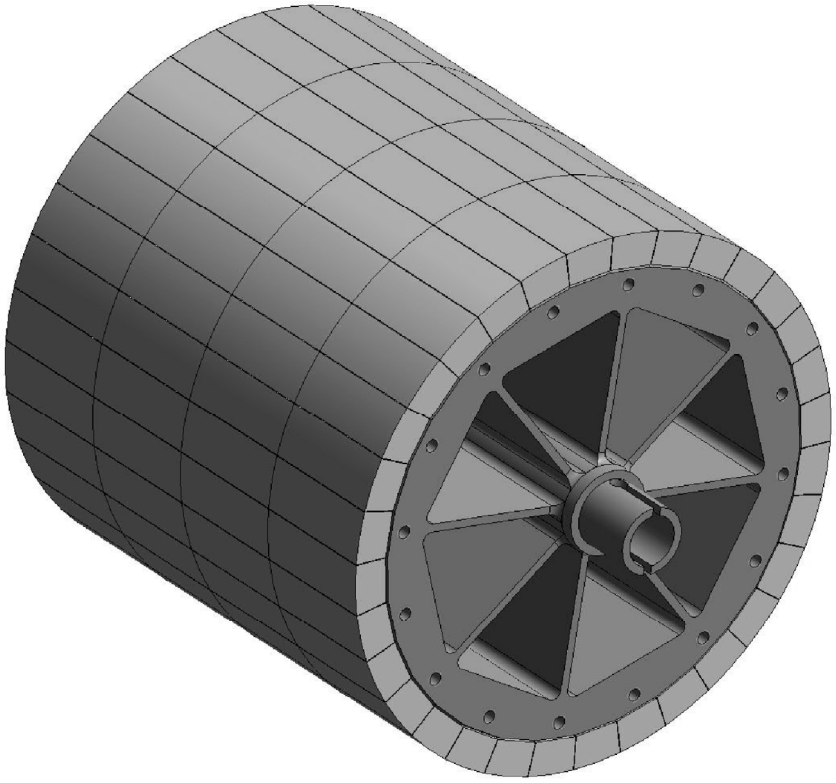

Figure 8.—Internal view of radial Halbach magnetic bearing rotor.

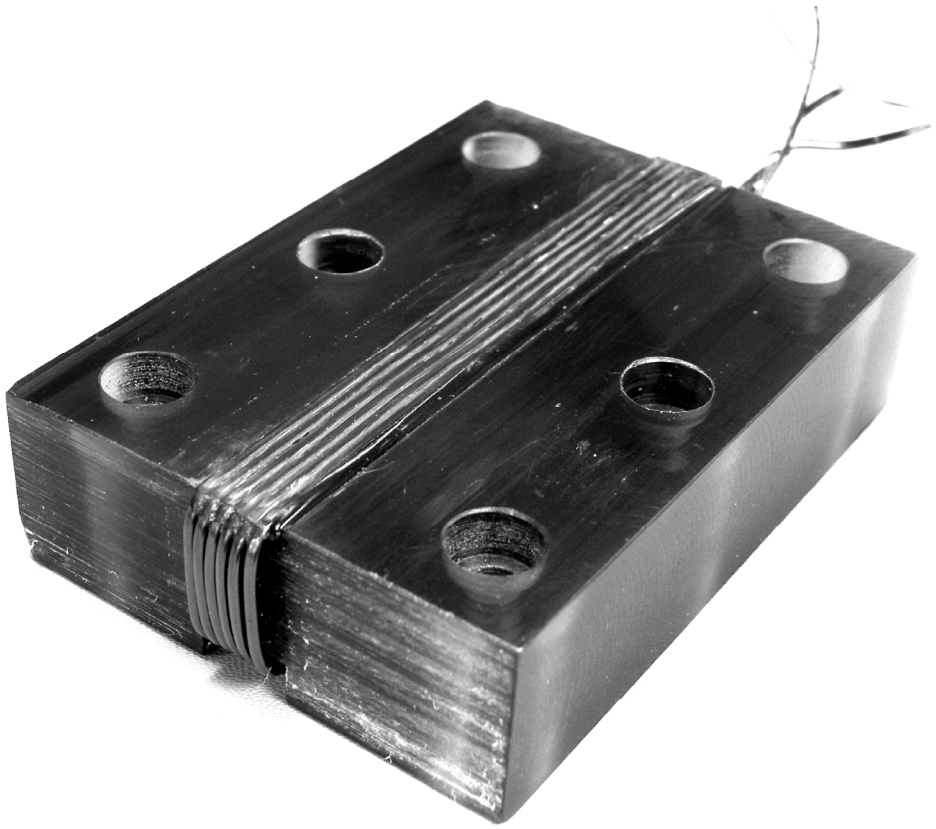

Figure 9.—Radial Halbach magnetic bearing test model r-z stator pole piece.

Four different stator pole pieces were tested. Two 4 in. *r-z* pole pieces were developed, one with one turn of wire, and the other with six turns of wire. Two 1 in. *r-z* pole pieces were developed, one with one turn of wire, and the other with six turns of wire. An *r-z* pole piece is shown in figure 9. All of the pole pieces have 20 gauge square copper magnet wire. The wire is wound around a slot in the pole piece machined from Ultem polyetherimide with a maximum operating temperature of 340 °F. The magnet wire is cemented in place in the slot to ensure that accurate data is obtained.

The pole piece may be terminated by an inductor to introduce a phase shift thus maximizing the generated repulsive force. Two different inductors were used; one consists of 17 turns of 14 gauge square copper wire wound around a ferrite rod, and the other has 27 turns of 20 gauge square copper wire wound around a ferrite rod.

The orientation of the pole piece is highly critical to maximize the force developed by the rotating rotor. The pole piece is connected with nylon fasteners to a precision horizontal linear stage which is connected to a precision vertical stage. These two stages allow for an accurate adjustment of the coil placement in close proximity to the surface of the rotor. The force measurement system monitors the force developed by the rotating rotor upon the pole piece.

Instrumentation

The Radial Halbach Magnetic Bearing Test Model was instrumented to measure bearing performance. Data from the drive motor, particularly rotor speed, were obtained from the motor drive system and sent directly to a personal computer (PC), where the data was stored. The other data were sent to the various test instruments and monitored. Test data includes stator pole piece voltage, stator pole piece current, stator pole piece force, stator pole piece temperature, and ambient temperature.

A block diagram of the instrumentation system is shown in figure 10. Type K thermocouples were used for all temperature measurements. Hall Effect transducers were used for all current measurements.

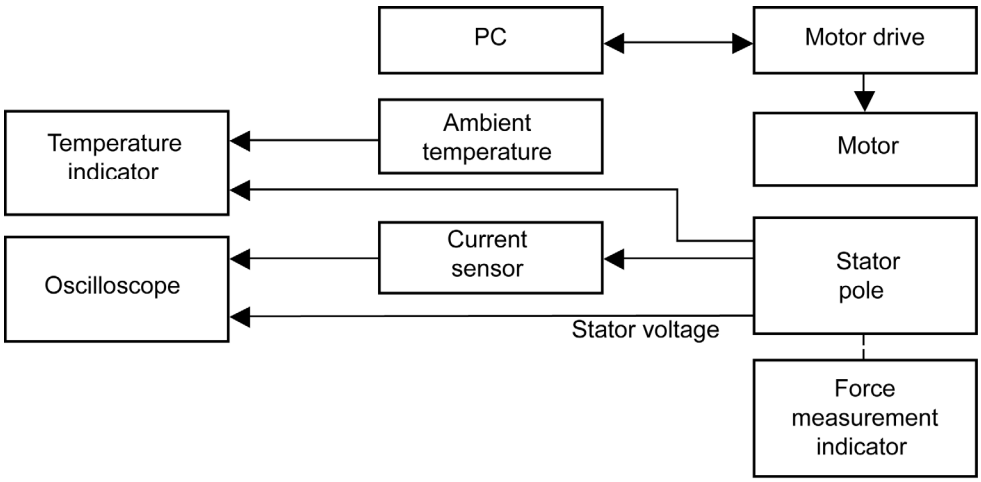

Figure 10.—Radial Halbach magnetic bearing instrumentation block diagram.

Test Procedures

The tests described in this report were conducted at the NASA Glenn Research Center in Cleveland, Ohio. The tests were conducted in accordance with the test matrix provided in Table 1.

Test models of the radial magnetic bearing with diameters of 4 in. and 1 in., respectively, validated the accuracy of the analytical model in the laboratory. The test procedure employed stators oriented in the *r-z* plane. The test matrix comprised stators with either a single turn winding or a 6-turn winding (i.e., N_t = 1 or N_t = 6). In the case of the 4 in. (102 mm) diameter test model, axial stator heights of *H* = 4 in. (102 mm) and *H* = 2 in. (51 mm) were tested. For the 1 in. (25 mm) diameter test model, only the H = 1 in. (25 mm) case was tested. All stators were wound with 20 AWG wire (d = 0.032 in. (0.8mm)).

The test consisted of precisely locating the stator beneath the magnet array such that the air gap was one of three selected values. For the 4 in. test model, the air gaps were 0.11 in. (2.8 mm), 0.16 in. (4.0 mm) and 0.21 in. (5.3 mm). Factoring in the thickness of the retaining shroud for the magnets and the finite radius of the conductor, the effective gap distances from the magnet surfaces to the center of the conductor were 0.196 in. (5.0 mm), 0.246 in. (6.2 mm) and 0.296 in. (7.5 mm), respectively. For the 1 in. test model the air gaps were 0.01 in. (0.25 mm), 0.025 in. (0.64 mm) and 0.04 in. (1.0 mm), resulting in effective gaps of 0.056 in. (1.4 mm), 0.071 in. (1.8 mm) and 0.086 in. (2.2 mm), respectively.

Peak-to-peak open circuit voltage (V_{oc}) and short circuit current (I_{ss}) were measured via oscilloscope with the rotor rotating at fixed mechanical speeds of 100, 250, 500, 1000, 2000 and 3000 rpm. The stator winding can accommodate a series inductor to provide the necessary phase shift between voltage and current to boost the production of lifting force. Two coils were included in these additional tests:

Coil 1: 17 turns, 14 AWG, L_c = 4.8 μH, R_c = 13.8 mΩ
Coil 2: 27 turns, 20 AWG, L_c = 77.4 μH, R_c = 34.6 mΩ

With these series coils inserted into the stator winding circuit, current (I_c) and lift force (F_{lift}) production were measured with the oscilloscope and a precision 200 gram scale, respectively.

The analytical model presented in this article predicted expected values for V_{oc}, I_{ss}, I_c and F_{lift}. Predicted values were compared to the measured results. Additionally, the analytical model predicted the drag force (F_{drag}) and power dissipation (P_d).

Finite element analysis (FEA) predictions at 1000 rpm were also compared to the analytical and measured results for V_{oc}, I_{ss}, I_c, F_{lift}, and F_{Drag}. Maxwell 3D software (Ansoft Corp., Pittsburgh, PA) generated the FEA predictions.

Table 1.—Radial Halbach magnetic bearing test matrix

Parameter	Stator (in.)	Gap (in.)	Speed (rpm)	Termination
4 in. single turn *r-z* stator pole	4 and 2 in.	0.110, 0.160, 0.210	100, 250, 500, 1000, 2000, 3000	Open circuit, short circuit, inductor
4 in. six turn *r-z* stator pole	4 and 2 in.	0.110, 0.160, 0.210	100, 250, 500, 1000, 2000, 3000	Open circuit, short circuit, inductor
1 in. single turn *r-z* stator pole	1 in.	0.010, 0.025, 0.040	100, 250, 500, 1000, 2000, 3000	Open circuit, short circuit, inductor
1 in. six turn *r-z* stator pole	1 in.	0.010, 0.025, 0.040	100, 250, 500, 1000, 2000, 3000	Open circuit, short circuit, inductor

Test Results

4-in. Test Model Results

Tables 2-5 summarize the results for the 4-in. radial test model. The tables include data for the analytical model, measured data and the FEA model, respectively. The data were obtained at 1000 rpm for three cases--the short circuit case and using the two series coils. A complete set of data for all rotational speeds is presented as a series of plots (A-1 through A-12) in the appendix.

Predicted and measured open circuit voltages generally agree within 5 percent for nearly all speeds in all three cases. At speeds of 1000 rpm or less, predicted and measured currents generally agree within 10 percent. At speeds above 1000 rpm, the predicted currents significantly exceed the measured values. In contrast, when using either series coil, the measured current significantly exceeds the predicted values at speeds above 1000 rpm. Predicted and measured values of lift force generally agree within 10 percent when using series coil #2. However, the predicted lift force significantly exceeds the measured values for the shorted winding, and the measured values significantly exceed the predicted value for series coil #1.

The greatest force production without a significant increase in temperature occurred with the 4-in. 6-Turn stator operating with the 0.11 in. air gap and series coil #2. Under these conditions, the model produced 0.151 kg-force at 3000 rpm with a lift/drag ratio of 2.4.

Of particular interest is the dependence of the generated lift force on the axial length, H, of the stator winding. Comparing the results for the H = 4 in. and H = 2 in. cases, note that doubling the axial length of the winding typically more than doubles the lift force produced. This effect is due to the fact that H linearly factors into both the flux calculation and the Lorentz force calculation. However, force production does not truly vary as H^2 since R and L are, respectively, linear and non-linear functions of H. Unfortunately, this same effect applies to the drag force as well, so the additional lift force comes with a price.

1-in. Test Model Results

Tables 6-7 summarize the induced voltage, current, lift force and power dissipation results for the 1-in. radial test model. The tables include data for the analytical model, measured data and the FEA model, respectively. The data were obtained at 1000 rpm for two cases--the short circuit case and using series coil #1. A more complete set of data for all rotational speeds is presented as a series of plots in the appendix (figs. A-13 through A-15). Lift forces were not measured, except at the very highest speeds.

As with the 4-in. model, the measured and predicted open circuit voltages generally agree within 5 percent. Predicted and measured currents agree within 10 percent up to 3000 rpm, at which point the same behaviors exhibited by the 4-in. test model appear, i.e., the predicted short circuit current exceeds the measured value, but the measured current with series coil #1 exceeds the predicted values.

Due to the unfavorable power factor and low amplitude of force production, complete lift force measurements were not taken on the 1-in. test model. However, when the model operated with a 0.010 in. air gap at 5000 rpm with series coil #1 inserted, it produced a measured lift force of 15.7 grams-force. This compared well with the analytically predicted value of 14.4 grams-force and the FEA-predicted value of 15.0 grams-force.

Table 2.—Comparison of analytically predicted, measured and FEA-predicted values at 1000 rpm for the 4 in. test model with a 4 in. by 1 in. stator winding of 6 turns. The stator resistance is R_s = 44.4 mΩ and the inductance is L_s = 4.8 μH. Values of peak-peak open circuit voltage (V_{oc}), peak-peak winding current (I), lift force (F_{Lift}), drag force (F_{Drag}) and real power dissipation (P_d) are given at three different air gaps (0.11, 0.16, and 0.21 in.) and with three different series combinations, including no series coil (R_c =0, L_c = 0, i.e., a shorted winding), Coil #1 (R_c = 13.8 mΩ, L_c = 4.8 μH) and Coil #2 (R_c = 34.6 mΩ, L_c = 77.4 μH). Measurement or analysis conditions that were not performed are left blank.

	4-in. radial test model at 1000 rpm, 4 in. by 1 in. stator, 6 turns								
	Air gap = 0.11 in. (2.8 mm), Eff. gap = 0.196 in. (5.0 mm)								
	No series coil			With series coil #1			With series coil #2		
Quantity	Analytical predicted	Measured	FEA predicted	Analytical predicted	Measured	FEA predicted	Analytical predicted	Measured	FEA predicted
V_{oc} (V)	1.97	2.00	2.04	1.97	2.00	2.04	1.97	2.00	2.04
I (A)	44.20	42.00	45.00	33.60	38.00	35.00	18.80	20.00	18.80
F_{lift} (N)	18.20	18.40	-------	21.00	40.10	51.00	56.50	53.20	61.00
F_{Drag} (N)	201.00	-------	-------	152.00	-------	150.00	64.80	-------	63.00
P_d (W)	21.50	-------	-------	16.10	-------	--------	3.97	-------	-------
	Air gap = 0.16 in. (4.0 mm), Eff. gap = 0.246 in. (6.2 mm)								
	No series coil			With series coil #1			With series coil #2		
	Analytical predicted	Measured	FEA predicted	Analytical predicted	Measured	FEA predicted	Analytical predicted	Measured	FEA predicted
V_{oc} (V)	1.64	1.70	1.77	1.64	1.70	1.77	1.64	1.70	1.77
I (A)	36.90	36.00	38.00	28.00	31.00	30.00	15.70	16.00	15.80
F_{lift} (N)	12.40	12.60	-------	14.30	28.40	38.00	38.50	37.60	46.00
F_{Drag} (N)	137.00	-------	-------	104.00	-------	102.00	44.20	-------	46.00
P_d (W)	15.00	-------	-------	11.20	-------	-------	2.76	-------	-------
	Air gap = 0.21 in. (5.3 mm), Eff. gap = 0.296 in. (7.5 mm)								
	No series coil			With series coil #1			With series coil #2		
	Analytical predicted	Measured	FEA predicted	Analytical predicted	Measured	FEA predicted	Analytical predicted	Measured	FEA predicted
V_{oc} (V)	1.38	1.40	1.44	1.38	1.40	1.44	1.38	1.40	1.44
I (A)	30.90	30.00	32.00	23.40	25.50	25.50	13.10	13.80	13.00
F_{lift} (N)	8.55	9.00	-------	9.84	20.90	20.00	26.50	25.60	30.00
F_{Drag} (N)	94.30	-------	-------	71.20	-------	70.00	30.40	-------	25.00
P_d (W)	10.50	-------	-------	7.83	-------	-------	1.93	-------	-------

Table 3.—Comparison of analytically predicted, measured and FEA-predicted values at 1000 rpm for the 4 in. test model with a 2 in. by 1 in. stator winding of 6 turns. The stator resistance is R_s = 30.6 mΩ and the inductance is L_s = 2.8 μH. Values of peak-peak open circuit voltage (V_{oc}), peak-peak winding current (I), lift force (F_{Lift}), drag force (F_{Drag}) and real power dissipation (P_d) are given at three different air gaps (0.11, 0.16, and 0.21 in.) and with three different series combinations, including no series coil (R_c =0, L_c = 0, i.e., a shorted winding), Coil #1 (R_c = 13.8 mΩ, L_c = 4.8 μH) and Coil #2 (R_c = 34.6 mΩ, L_c = 77.4 μH). Measurement or analysis conditions that were not performed are left blank.

	4-in. radial test model at 1000 rpm, 2 in. by 1 in. stator, 6 turns								
	Air gap = 0.11 in. (2.8 mm), Eff. gap = 0.196 in. (5.0 mm)								
	No series coil			With series coil #1			With series coil #2		
Quantity	Analytical predicted	Measured	FEA predicted	Analytical predicted	Measured	FEA predicted	Analytical predicted	Measured	FEA predicted
V_{oc} (V)	1.19	1.15	1.16	1.19	1.15	1.16	1.19	1.15	1.16
I (A)	38.60	32.00	31.20	26.40	28.00	25.00	12.70	12.00	11.60
F_{lift} (N)	8.00	6.10	-------	10.28	21.10	19.00	24.20	20.50	20.00
F_{Drag} (N)	105.6	-------	-------	71.70	-------	60.00	24.90	-------	18.00
P_d (W)	11.34	-------	-------	7.59	-------	-------	1.27	-------	-------
	Air gap = 0.16 in. (4.0 mm), Eff. gap = 0.246 in. (6.2 mm)								
	No series coil			With series coil #1			With series coil #2		
	Analytical predicted	Measured	FEA predicted	Analytical predicted	Measured	FEA predicted	Analytical predicted	Measured	FEA predicted
V_{oc} (V)	0.99	0.98	0.97	0.99	0.98	0.97	0.99	0.98	0.97
I (A)	32.20	29.00	30.00	22.00	25.00	20.80	10.60	10.00	9.60
F_{lift} (N)	5.52	4.77	-------	7.01	15.80	13.80	16.50	14.70	15.30
F_{Drag} (N)	72.00	-------	-------	48.90	-------	45.00	17.00	-------	13.00
P_d (W)	7.88	-------	-------	5.28	-------	-------	0.88	-------	-------
	Air gap = 0.21 in. (5.3 mm), Eff. gap = 0.296 in. (7.5 mm)								
	No series coil			With series coil #1			With series coil #2		
	Analytical predicted	Measured	FEA predicted	Analytical predicted	Measured	FEA predicted	Analytical predicted	Measured	FEA predicted
V_{oc} (V)	0.83	0.80	0.80	0.83	0.80	0.80	0.83	0.80	0.80
I (A)	26.90	25.00	25.00	18.40	20.00	17.50	8.83	8.20	8.10
F_{lift} (N)	3.80	3.60	-------	4.82	11.70	10.00	11.70	9.80	10.00
F_{Drag} (N)	49.5	-------	-------	33.60	-------	27.00	11.30	-------	9.50
P_d (W)	5.52	-------	-------	3.70	-------	-------	0.62	-------	-------

Table 4.—Comparison of analytically predicted, measured and FEA-predicted values at 1000 rpm for the 4 in. test model with a 4 in. x 1 in. stator winding of 1 turn. The stator resistance is R_s = 12.7 mΩ and the inductance is L_s = 0.55 μH. Values of peak-peak open circuit voltage (V_{oc}), peak-peak winding current (I), lift force (F_{Lift}), drag force (F_{Drag}) and real power dissipation (P_d) are given at three different air gaps (0.11, 0.16, and 0.21 in.) and with three different series combinations, including no series coil (R_c =0, L_c = 0, i.e., a shorted winding), Coil #1 (R_c = 13.8 mΩ, L_c = 4.8 μH) and Coil #2 (R_c = 34.6 mΩ, L_c = 77.4 μH). Measurement or analysis conditions that were not performed are left blank.

	4-in. radial test model at 1000 rpm, 4 in. by 1 in. stator, 1 turn								
	Air gap = 0.11 in. (2.8 mm), Eff. gap = 0.196 in. (5.0 mm)								
	No series coil			With series coil #1			With series coil #2		
Quantity	Analytical predicted	Measured	FEA predicted	Analytical predicted	Measured	FEA predicted	Analytical predicted	Measured	FEA predicted
V_{oc} (V)	0.34	0.36	0.37	0.34	0.36	0.37	0.34	0.36	0.37
I (A)	26.80	24.50	28.00	12.70	15.50	13.30	4.23	4.20	4.30
F_{lift} (N)	0.77	-------	-------	1.67	6.60	4.00	2.70	3.33	3.20
F_{Drag} (N)	21.1	-------	-------	9.88	-------	10.00	1.96	-------	1.50
P_d (W)	2.28	-------	-------	1.04	-------	-------	0.07	-------	-------
	Air gap = 0.16 in. (4.0 mm), Eff. gap = 0.246 in. (6.2 mm)								
	No series coil			With series coil #1			With series coil #2		
	Analytical predicted	Measured	FEA predicted	Analytical predicted	Measured	FEA predicted	Analytical predicted	Measured	FEA predicted
V_{oc} (V)	0.29	0.30	0.31	0.29	0.30	0.31	0.29	0.30	0.31
I (A)	22.30	22.00	24.00	10.60	12.20	11.20	3.52	3.75	3.70
F_{lift} (N)	0.52	-------	-------	1.13	4.90	2.30	1.84	2.50	2.30
F_{Drag} (N)	14.37	-------	-------	6.70	-------	7.00	1.33	-------	1.10
P_d (W)	1.58	-------	-------	0.72	-------	-------	0.05	-------	-------
	Air gap = 0.21 in. (5.3 mm), Eff. gap = 0.296 in. (7.5 mm)								
	No series coil			With series coil #1			With series coil #2		
	Analytical predicted	Measured	FEA predicted	Analytical predicted	Measured	FEA predicted	Analytical predicted	Measured	FEA predicted
V_{oc} (V)	0.24	0.25	0.25	0.24	0.25	0.25	0.24	0.25	0.25
I (A)	18.60	17.50	19.50	8.82	11.00	9.20	2.94	3.00	3.10
F_{lift} (N)	0.36	-------	-------	0.78	3.60	1.00	1.26	1.04	1.30
F_{Drag} (N)	9.85	-------	-------	4.60	-------	4.50	0.91	-------	1.00
P_d (W)	1.10	-------	-------	0.50	-------	-------	0.03	-------	-------

Table 5.—Comparison of analytically predicted, measured and FEA-predicted values at 1000 rpm for the 4 in. test model with a 2 in. by 1 in. stator winding of 1 turn. The stator resistance is R_s = 8.6 mΩ and the inductance is L_s = 0.38 μH. Values of peak-peak open circuit voltage (V_{oc}), peak-peak winding current (I), lift force (F_{Lift}), drag force (F_{Drag}) and real power dissipation (P_d) are given at three different air gaps (0.11, 0.16, and 0.21 in.) and with three different series combinations, including no series coil (R_c =0, L_c = 0, i.e., a shorted winding), Coil #1 (R_c = 13.8 mΩ, L_c = 4.8 μH) and Coil #2 (R_c = 34.6 mΩ, L_c = 77.4 μH). Measurement or analysis conditions that were not performed are left blank.

	4-in. radial test model at 1000 rpm, 2 in. by 1 in. stator, 1 turn								
	Air gap = 0.11 in. (2.8 mm), Eff. gap = 0.196 in. (5.0 mm)								
	No series coil			With series coil #1			With series coil #2		
Quantity	Analytical predicted	Measured	FEA predicted	Analytical predicted	Measured	FEA predicted	Analytical predicted	Measured	FEA predicted
V_{oc} (V)	0.20	0.20	0.20	0.20	0.20	0.20	0.20	0.20	0.20
I (A)	22.60	21.00	22.70	8.54	9.00	8.40	2.49	2.50	2.40
F_{lift} (N)	0.38	-------	-------	0.73	-------	1.02	0.94	0.97	0.80
F_{Drag} (N)	10.22	-------	-------	3.79	-------	3.40	0.62	-------	0.45
P_d (W)	1.10	-------	-------	0.39	-------	-------	0.02	-------	-------
	Air gap = 0.16 in. (4.0 mm), Eff. gap = 0.246 in. (6.2 mm)								
	No series coil			With series coil #1			With series coil #2		
	Analytical predicted	Measured	FEA predicted	Analytical predicted	Measured	FEA predicted	Analytical predicted	Measured	FEA predicted
V_{oc} (V)	0.32	0.33	0.16	0.16	0.16	0.16	0.16	0.16	0.16
I (A)	37.60	34.00	18.50	7.11	8.40	7.00	2.08	2.10	2.00
F_{lift} (N)	0.26	-------	-------	0.50	-------	0.80	0.64	0.77	0.60
F_{Drag} (N)	6.95	-------	-------	2.57	-------	2.30	0.42	-------	0.35
P_d (W)	0.76	-------	-------	0.27	-------	-------	0.01	-------	-------
	Air gap = 0.21 in. (5.3 mm), Eff. gap = 0.296 in. (7.5 mm)								
	No series coil			With series coil #1			With series coil #2		
	Analytical predicted	Measured	FEA predicted	Analytical predicted	Measured	FEA predicted	Analytical predicted	Measured	FEA predicted
V_{oc} (V)	0.41	0.42	0.14	0.14	0.14	0.14	0.14	0.14	0.14
I (A)	47.00	40.00	16.00	5.95	7.20	6.00	1.73	1.90	1.70
F_{lift} (N)	0.18	-------	-------	0.34	-------	0.50	0.44	0.42	0.40
F_{Drag} (N)	4.76	-------	-------	1.76	-------	1.70	0.29	-------	0.25
P_d (W)	0.53	-------	-------	0.19	-------	-------	0.01	-------	-------

Table 6.—Comparison of analytically predicted, measured and FEA-predicted values at 1000 rpm for the 1 in. test model with a 1 in. by 1 in. stator winding of 6 turns. The stator resistance is R_s = 21.0 mΩ and the inductance is L_s = 1.75 μH. Values of peak-peak open circuit voltage (V_{oc}), peak-peak winding current (I), lift force (F_{Lift}), and real power dissipation (P_d) are given at three different air gaps (0.010, 0.025, and 0.040 in.) and with three different series combinations, including no series coil (R_c =0, L_c = 0, i.e., a shorted winding), Coil #1 (R_c = 13.8 mΩ, L_c = 4.8 μH) and Coil #2 (R_c = 34.6 mΩ, L_c = 77.4 μH). Measurement or analysis conditions that were not performed are left blank.

	1-in. radial test model at 1000 rpm, 1 in. by 1 in. stator, 6 turns					
	Air gap = 0.01 in. (0.25 mm), Eff. gap = 0.056 in. (1.42 mm)					
	No series coil			With series coil #1		
Quantity	Analytical predicted	Measured	FEA predicted	Analytical predicted	Measured	FEA predicted
V_{oc} (V)	0.16	0.16	0.15	0.16	0.16	0.15
I (A)	7.79	7.80	7.00	7.25	6.50	-------
F_{lift} (grams-force)	0.039	-------	-------	0.64	-------	-------
P_d (W)	0.32	-------	-------	0.26	-------	-------
	Air gap = 0.025 in. (0.64 mm), Eff. gap = 0.071 in. (1.8 mm)					
	No series coil			With series coil #1		
	Analytical predicted	Measured	FEA predicted	Analytical predicted	Measured	FEA predicted
V_{oc} (V)	0.30	0.30	0.14	0.15	0.14	0.14
I (A)	14.05	13.00	6.40	6.60	6.00	-------
F_{lift} (grams-force)	0.031	-------	-------	0.51	-------	-------
P_d (W)	0.26	-------	-------	0.21	-------	-------
	Air gap = 0.04 in. (1.02 mm), Eff. gap = 0.086 in. (2.2 mm)					
	No series coil			With series coil #1		
	Analytical predicted	Measured	FEA predicted	Analytical predicted	Measured	FEA predicted
V_{oc} (V)	0.40	0.40	0.12	0.13	0.13	0.12
I (A)	19.00	18.00	5.70	5.95	5.50	-------
F_{lift} (grams-force)	0.025	-------	-------	0.41	-------	-------
P_d (W)	0.21	-------	-------	0.18	-------	-------

Table 7.—Comparison of analytically predicted, measured and FEA-predicted values at 1000 rpm for the 1 in. test model with a 1 in. by 1 in. stator winding of 1 turn. The stator resistance is R_s = 10.3 mΩ and the inductance is L_s = 0.17 μH. Values of peak-peak open circuit voltage (V_{oc}), peak-peak winding current (I), lift force (F_{Lift}), and real power dissipation (P_d) are given at three different air gaps (0.010, 0.025, and 0.040 in.) and with three different series combinations, including no series coil (R_c =0, L_c = 0, i.e., a shorted winding), Coil #1 (R_c = 13.8 mΩ, L_c = 4.8 μH) and Coil #2 (R_c = 34.6 mΩ, L_c = 77.4 μH). Measurement or analysis conditions that were not performed are left blank.

	1-in. radial test model at 1000 rpm, 1 in. by 1 in. stator, 1 turn		
	Air gap = 0.01 in. (0.25 mm), Eff. gap = 0.056 in. (1.42 mm)		
	No series coil		
Quantity	Analytical predicted	Measured	FEA predicted
V_{oc} (V)	0.03	0.03	0.03
I (A)	3.07	2.60	2.70
F_{lift} (grams-force)	0.006	-------	-------
P_d (W)	0.024	-------	-------
	Air gap = 0.025 in. (0.64 mm), Eff. gap = 0.071 in. (1.8 mm)		
	No series coil		
	Analytical predicted	Measured	FEA predicted
V_{oc} (V)	0.06	0.05	0.03
I (A)	5.51	4.80	2.44
F_{lift} (grams-force)	0.005	-------	-------
P_d (W)	0.020	-------	-------
	Air gap = 0.04 in. (1.02 mm), Eff. gap = 0.086 in. (2.2 mm)		
	No series coil		
	Analytical predicted	Measured	FEA predicted
V_{oc} (V)	0.08	0.07	0.02
I (A)	7.46	6.60	2.28
F_{lift} (grams-force)	0.004	-------	-------
P_d (W)	0.016	-------	-------

Discussion

The excellent agreement between measured and predicted open circuit voltages validates the analytical equations for the magnetostatic field and induced EMF as a function of rotor and stator geometries, magnet properties, winding factor and air gap. Good agreement between measured and predicted currents and forces at low speeds further validates the dynamic equations of the analytical model. Additional physical effects explain the discrepancies observed at higher speeds as discussed below.

The drop in measured current (vs. predicted) at higher rotational speeds arises from an increase in winding resistance due to higher temperature (ref. 3). For example, a 30° rise in temperature will increase the stator resistance by 10 percent. Measured temperature increases sometimes exceeded 50 °C with the 4-in. test model operating at the smallest air gap.

The rise in measured current (vs. predicted) when using a series coil arises from saturation of the inductor core at high currents (ref. 4). Under saturation conditions, the inductance drops and the coil no longer behaves as a true inductor (i.e., impedance no longer rises linearly with frequency). This effect also produces harmonic distortion of the normally sinusoidal current waveform as observed on the oscilloscope.

These same physical phenomena translate to the production of the lift force, which scales linearly with winding current. Additionally, eddy currents in the larger gauge wire of series coil #1 may further contribute to the rather large discrepancy (~100 percent) observed between the measured and predicted values of lift force for this coil. This effect is apparently ameliorated by the lower diameter winding of series coil #2.

In summary, the analytical model presented in this paper may be considered valid under the following conditions:

a) The temperature rise in the stator winding remains less than 10 °C.
b) The electrical frequency of the system is kept low enough so that the skin depth on the stator winding conductor is not small compared to the conductor diameter. This condition must be evaluated for a given design.
c) If a ferrite core inductor is used to produce a favorable power factor for force production, the currents must be kept low enough so as not to saturate the core. This condition must be evaluated for the specific inductor used.
d) The stator winding conductor diameter is kept sufficiently small to preclude the development of eddy currents under the strong time-varying magnetic fields of the Halbach array. This condition must be verified for the particular choice of stator winding conductor.

Concluding Remarks

The NASA John H. Glenn Research Center has successfully designed, developed, analyzed, and tested a revolutionary Radial Halbach Magnetic Bearing. The goals of the program include improving aircraft efficiency, reliability, and safety. The objective of this work is to develop a viable non-contact magnetic bearing utilizing Halbach arrays for all-electric flight, and many other applications. This concept will help to reduce harmful emissions, reduce the Nation's dependence on fossil fuels and mitigate many of the concerns and limitations encountered in conventional axial bearings such as bearing wear, leaks, seals and friction loss. The Radial Halbach Magnetic Bearing is inherently stable and requires no active feedback control system or superconductivity as required in many magnetic bearing designs. The Radial Halbach Magnetic Bearing is useful for very high speed applications where conventional bearings cannot be used including turbines, instrumentation, and medical applications.

Theoretical derivations have been developed successfully to predict the levitation forces generated by a circular Halbach array and coil assembly. Finite element analyses successfully validated the theoretical derivations. Empirical test results obtained from experimental hardware successfully validated the basic principles described, and the theoretical work that was performed. Of particular value, are the analytical tools and capability that were developed successfully under this project. Performance predictions can be made confidently for machines of various scale.

The test results were obtained using a small scale test model. The factors limiting performance of this model improve significantly when the physical scale is increased. For large machines on the order of 1 m diameter, the stator inductance to resistance ratio may be made favorable enough to make the use of an external series inductor unnecessary, even at speeds of less than 1000 rpm. This favorable balance results in less resistive heating and the larger size gives more thermal mass, as well as more surface area from which to radiate heat.

The report concludes that the implementation of Radial Halbach Magnetic Bearings is feasible and can provide significant improvements in rotational system performance and reliability. In addition to aircraft engines, this technology has potential application in ultra-efficient motors, computer memory systems, instrumentation systems, medical systems, manufacturing equipment, and space power systems, such as generators and flywheels.

References

1. Halbach, Klaus, “Application of Permanent Magnets in Accelerators and Electron Storage Rings,” Journal of Applied Physics, vol. 57, no. 1, pp. 3605–3608, (April 1985)
2. Post, R.F., Ryutov, D.D., “Ambient-Temperature Passive Magnetic Bearings: Theory and Design Equations,” Proceedings of the Sixth International Symposium on Magnetic Bearings, pp. 110–122, (1998)
3. Serway, Raymond A. (1998). *Principles of Physics*, 2nd ed., Fort Worth, TX; London: Saunders College Pub.
4. Van den Bossche, A. and Valchev, V.C. *Inductors and Transformers for Power Electronics*, Boca Raton, FL: Taylor and Francis Publ. Grp.

Appendix A—Equipment Under Test Summary Data Sheet

1.0 Radial Halbach Magnetic Bearing Test Model

1.1 1 in. Test Model Drive Motor

1.1.1	Type	Brushless DC Servomotor
1.1.2	DC Voltage Range	20 to 48 V
1.1.3	Operating Temperature	0 to 70 °C (32 to 158 °F)
1.1.4	Storage Temperature	–20 to 85°C (–4 to 185 °F)
1.1.5	Humidity	0 to 80 percent
1.1.6	Peak Torque	0.63 N-m (89 oz-in.)
1.1.7	Continuous Torque	0.24 N-m (33 oz-in.)
1.1.8	No Load Speed	7400 rpm
1.1.9	Nominal Power	0.10 kW (0.14 hp)
1.1.10	Servo Update	4069 Hz
1.1.11	Rotor Inertia	1.34×10^{-5} kg-m^2 (0.0019 oz-in^2)
1.1.12	Width	57.2 mm (2.25 in.)
1.1.13	Length	115 mm (4.5 in.)
1.1.14	Weight	0.95 kg (2.1 lb)

1.2 4 in. Test Model Drive Motor

1.2.1	Type	AC Servomotor
1.2.2	Voltage	200 V
1.2.3	Operating Temperature	0 to 40 °C (32 to 104 °F)
1.2.4	Peak Torque	14.68 N-m (130 in-lb)
1.2.5	Rated Torque	4.85 N-m (43 in-lb)
1.2.6	Rated Speed	3000 rpm
1.2.7	Maximum Speed	5000 rpm
1.2.8	Nominal Power	1.5 kW (2.0 hp)
1.2.9	Rotor Inertia	0.25 N-m-s$^2 \times 10^{-3}$ (2.19 in-lb-s$^2 \times 10^{-3}$)

1.3 Force Measurement System

1.3.1	Type	Variable Capacitance
1.3.2	Capacity	410 g
1.3.3	Readability	0.001 g
1.3.4	Linearity	± 0.02 g

2.0 1 in. Test Model Rotor

2.1	Diameter	2.69 cm (1.06 in)
2.2	Length	2.89 cm (1.14 in)
2.3	Weight	94 g (0.21 lb)
2.4	Magnet Type	Neodymium Iron Boron B55
2.5	Magnet Orientation	Halbach Array (32)
2.6	Magnet Shape	Sectors

3.0 4 in. Test Model Rotor

3.1	Diameter	10.54 cm (4.15 in)
3.2	Length	10.95 cm (4.31 in)
3.3	Weight	2800 g (6.2 lb)
3.4	Magnet Type	Neodymium Iron Boron B55
3.5	Magnet Orientation	Halbach Array (16)
3.6	Magnet Shape	Sectors

4.0 1 in. Test Model Single Turn 1 in. *r-z* Stator Pole Piece

4.1	Wire	#20 Square Copper
4.2	Inductance	0.17 μH
4.3	Resistance	10.30 mΩ

5.0. 1 in. Test Model Six Turn 1 in. *r-z* Stator Pole Piece

5.1	Wire	#20 Square Copper
5.2	Inductance	1.75 μH
5.3	Resistance	21.0 mΩ

6.0 4 in. Test Model Single Turn 4 in. *r-z* Stator Pole Piece

6.1	Wire	#20 Square Copper
6.2	Inductance	0.55 μH
6.3	Resistance	12.7 mΩ

7.0 4 in. Test Model Six Turn 4 in. *r-z* Stator Pole Piece

7.1	Wire	#20 Square Copper
7.2	Inductance	4.8 μH
7.3	Resistance	44.4 mΩ

8.0 4 in. Test Model Single Turn 2 in. *r-z* Stator Pole Piece

8.1	Wire	#20 Square Copper
8.2	Inductance	0.38 μH
8.3	Resistance	8.6 mΩ

9.0 4 in. Test Model Six Turn 2 in. *r-z* Stator Pole Piece

9.1	Wire	#20 Square Copper
9.2	Inductance	2.8 μH
9.3	Resistance	30.6 mΩ

10.0 Inductor No. 1

10.1	Configuration	Helix
10.2	Wire	#14 Square Copper
10.3	Number of Turns	17
10.4	Core	Ferrite Rod
10.5	Inductance	4.8 μH
10.6	Resistance	13.8 mΩ

11.0 Inductor No. 2

11.1	Configuration	Helix
11.2	Wire	#20 Square Copper
11.3	Number of Turns	27
11.4	Core	Ferrite Rod
11.5	Inductance	77.4 μH
11.6	Resistance	34.6 mΩ

Appendix B—System Performance Test Results

A complete set of plots of the test results are included here. Table 1 identifies the tests that were conducted.

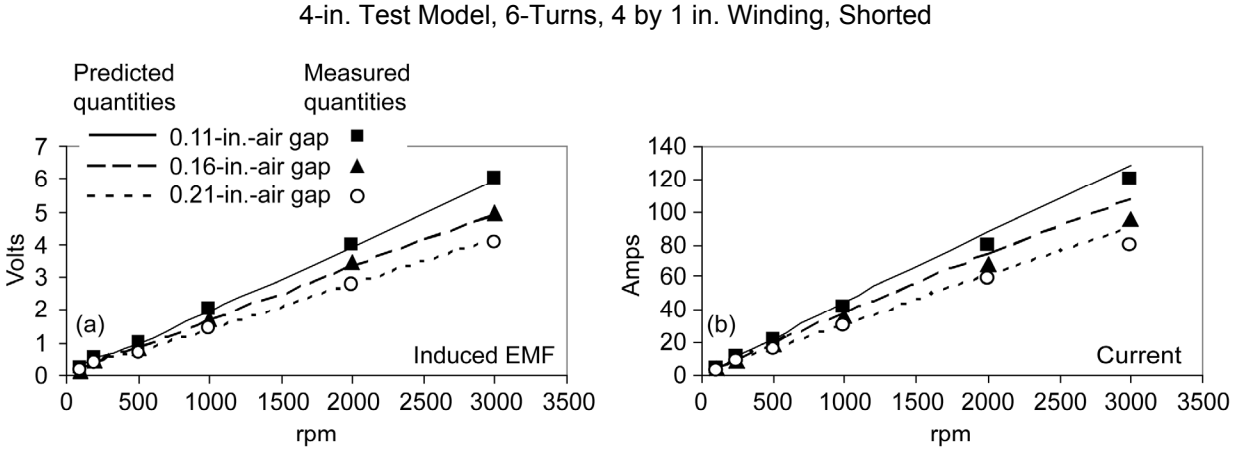

Figure A–1.—Plots of analytically predicted and measured quantities versus rpm for 4-in.-radial test model stator winding, including (a) induced EMF in volts, (b) current in amps. Stator winding is six turns of 20 AWG, H = 4 in., W = 1 in., R_s = 44.4 mΩ, L_s = 4.8 μH, with no series inductor: R_c = 0, L_c = 0.

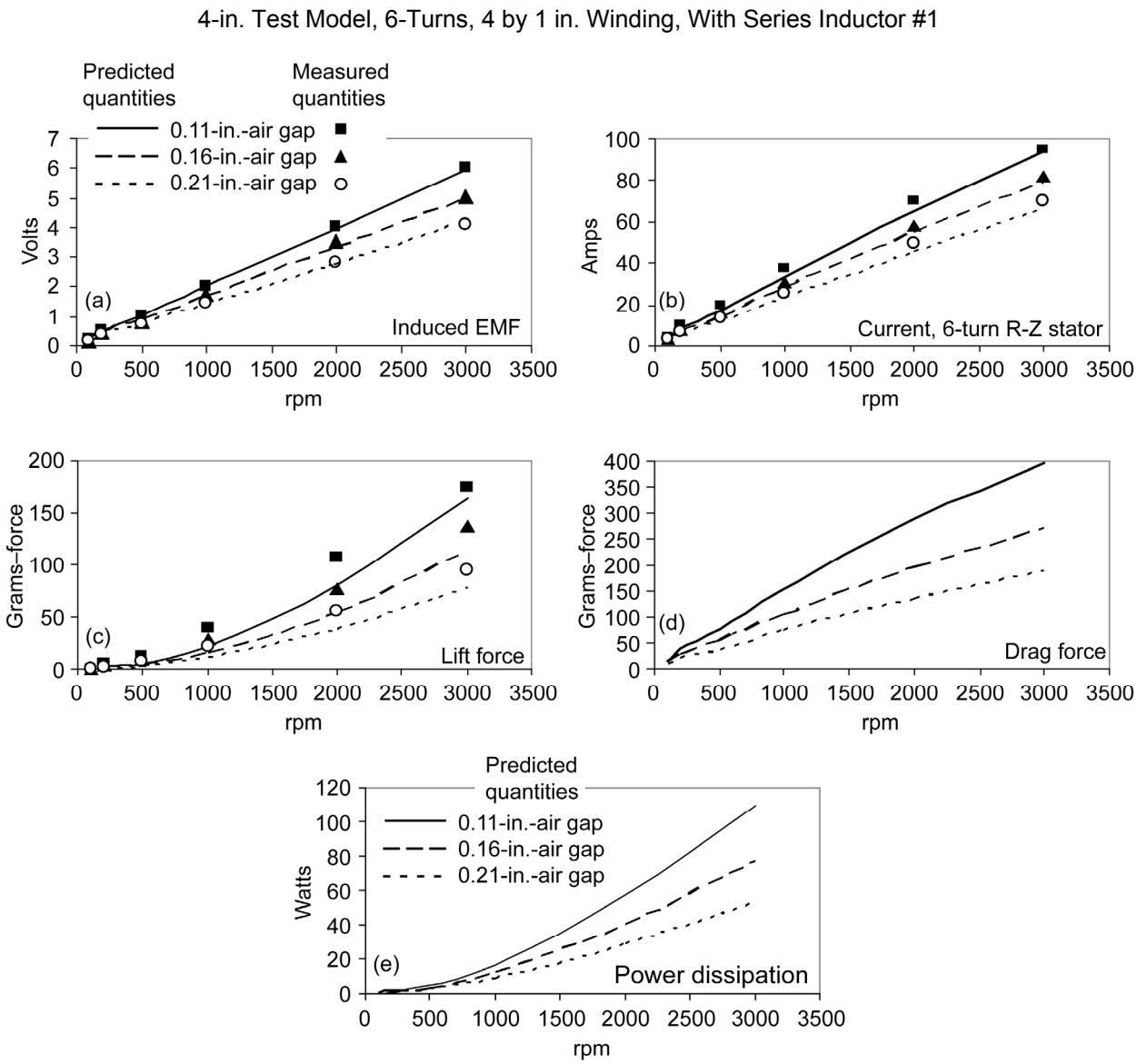

Figure A–2.—Plots of analytically predicted versus measured quantities for 4-in.-radial test model stator winding, including induced EMF in volts (a), current in amps (b), and lift force in grams–force (c). Predicted values only for drag force in grams–force (d) and power dissipation in watts (e). Stator winding is six turns of 20 AWG, H = 4 in., W = 1 in., R_s = 44.4 mΩ, L_s = 4.8 μH, with series inductor 1: R_c = 13.8 mΩ, L_c = 4.8 μH.

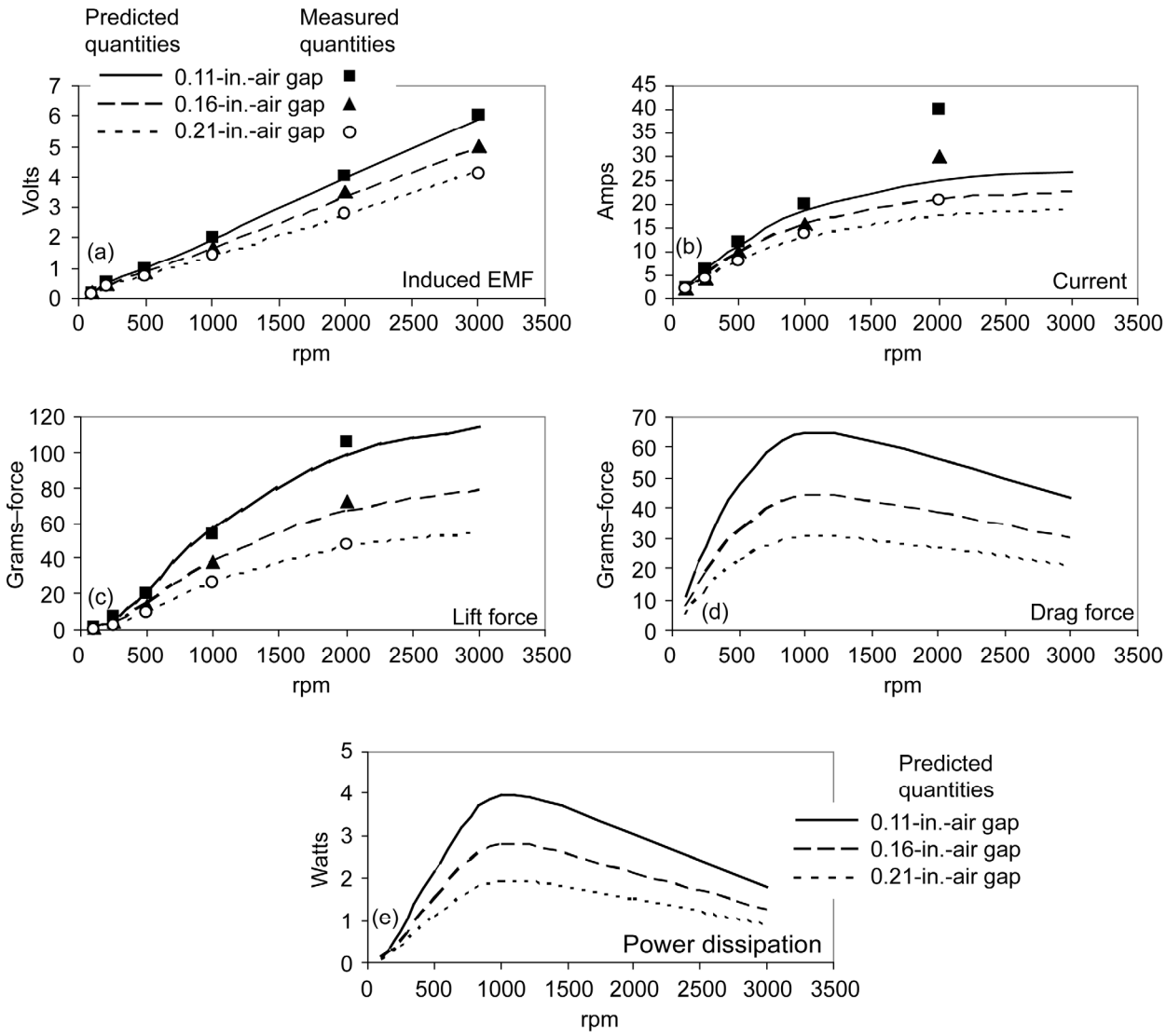

Figure A–3.—Plots of analytically predicted versus measured quantities for 4-in.-radial test model stator winding, including induced EMF in volts (a), current in amps (b), and lift force in grams–force (c). Predicted values only for drag force in grams–force (d) and power dissipation in watts (e). Stator winding is six turns of 20 AWG, H = 4 in., W = 1 in., R_s = 44.4 mΩ, L_s = 4.8 μH, with series inductor 1: R_c = 34.6 mΩ, L_c = 77.4 μH. Note the effects of inductor core saturation on the measured current in (b) above 1500 rpm.

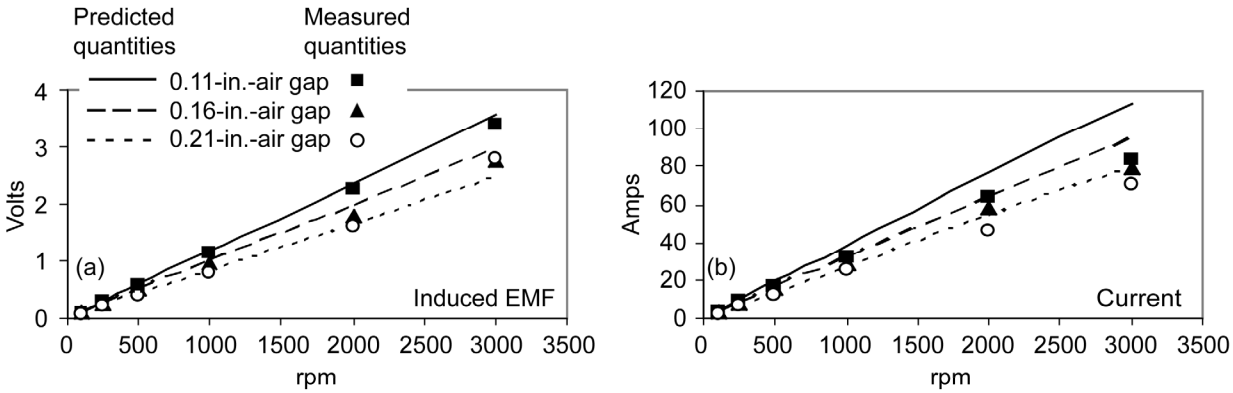

Figure A–4.—Plots of analytically predicted and measured quantities versus rpm for 2-in.-radial test model stator winding, including induced EMF in volts (a), current in amps (b). Stator winding is six turns of 20 AWG, H = 2 in., W = 1 in., R_s = 30.6 mΩ, L_s = 2.8 μH, with no series inductor: R_c = 0, L_c = 0.

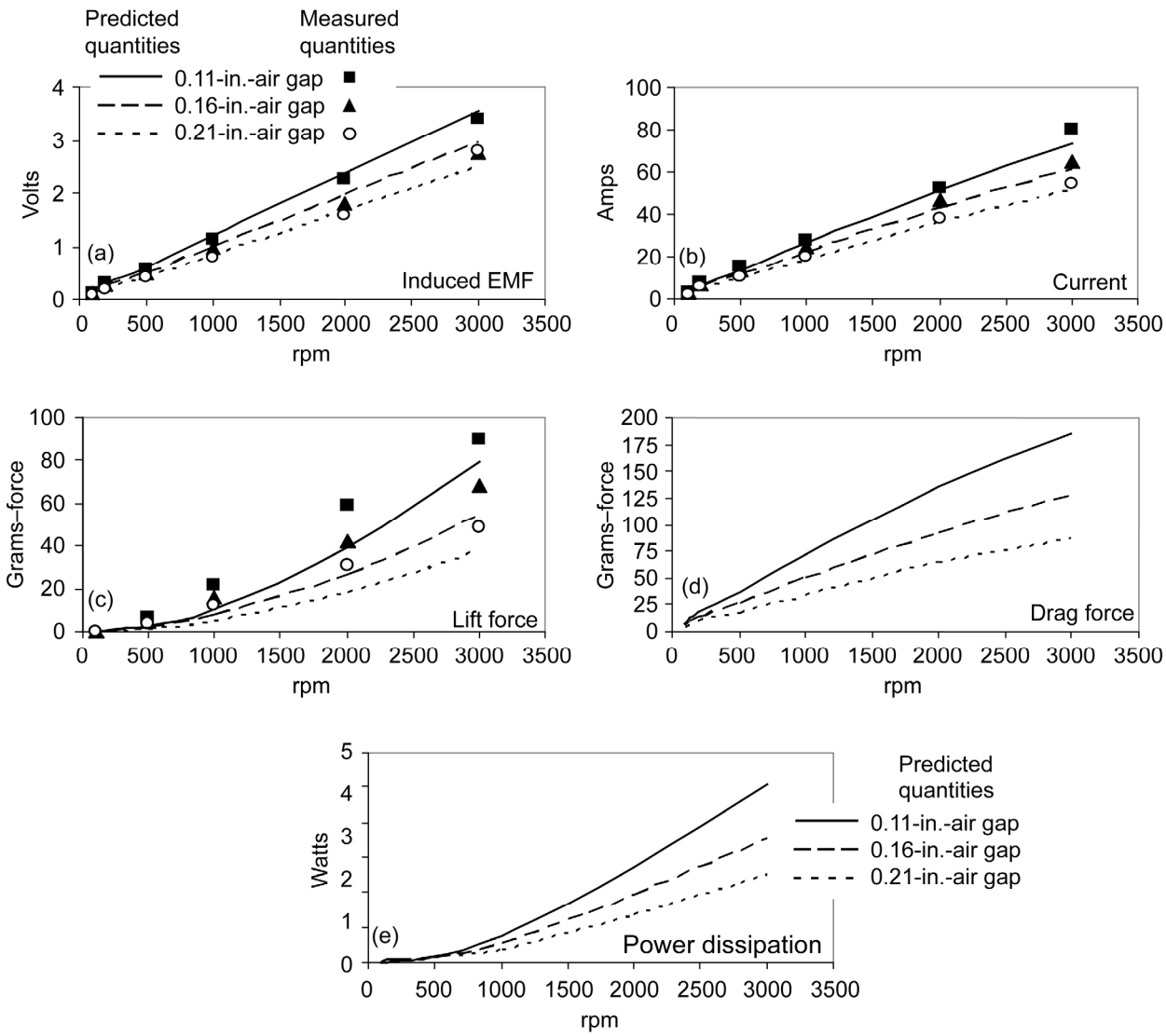

Figure A–5.—Plots of analytically predicted versus measured quantities for 4-in.-radial test model stator winding, including induced EMF in volts (a), current in amps (b), and lift force in grams–force (c). Predicted values only for drag force in grams–force (d) and power dissipation in watts (e). Stator winding is six turns of 20 AWG, H = 2 in., W = 1 in., R_s = 30.6 mΩ, L_s = 2.8 μH, with series inductor 1: R_c = 13.8 mΩ, L_c = 4.8 μH.

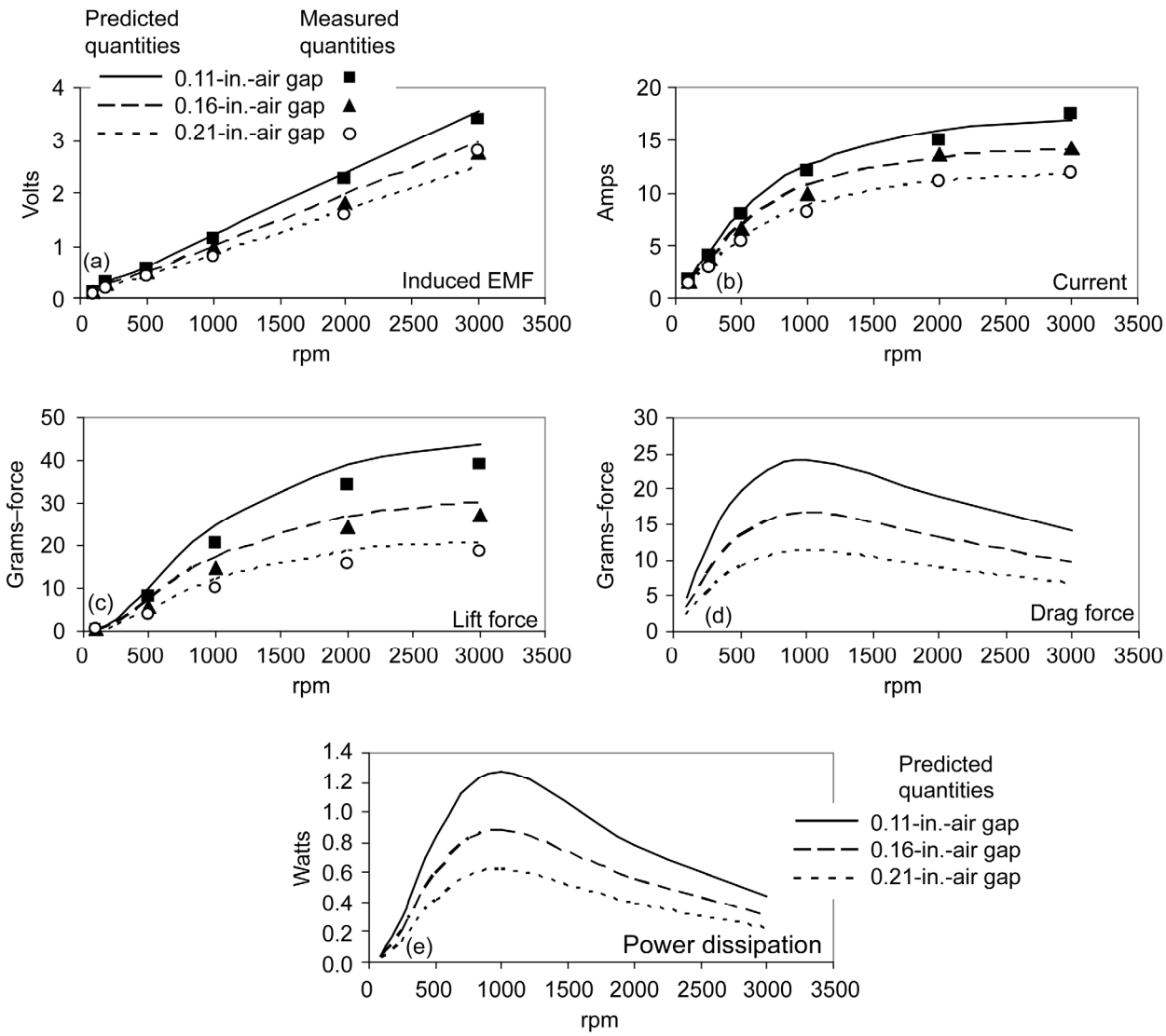

Figure A–6.—Plots of analytically predicted versus measured quantities for 4-in.-radial test model stator winding, including induced EMF in volts (a), current in amps (b), and lift force in grams–force (c). Predicted values only for drag force in grams–force (d) and power dissipation in watts (e). Stator winding is six turns of 20 AWG, H = 2 in., W = 1 in., R_s = 30.6 mΩ, L_s = 2.8 μH, with series inductor 2: R_c = 34.6 mΩ, L_c = 77.4 μH.

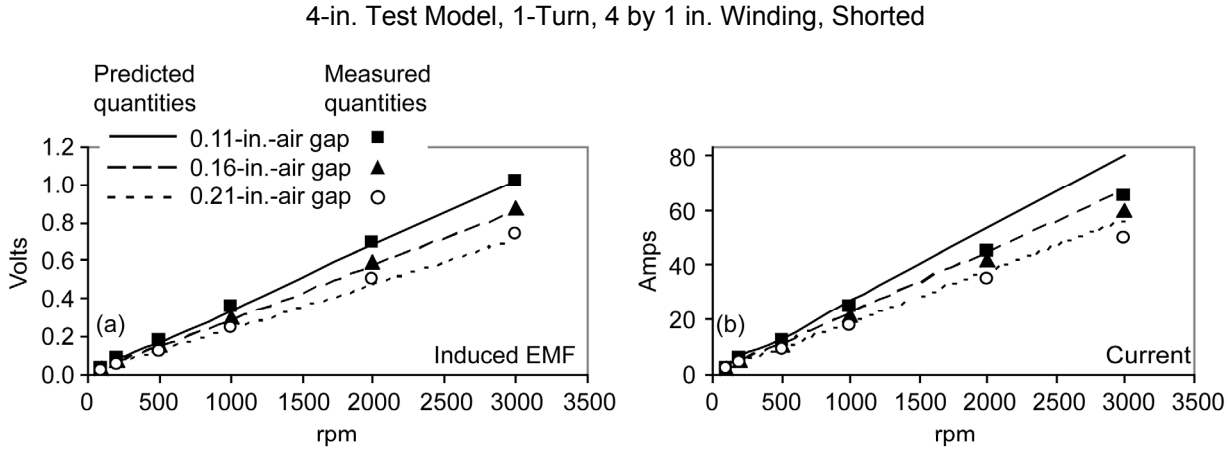

Figure A–7.—Plots of analytically predicted and measured quantities versus rpm for 2-in.-radial test model stator winding, including induced EMF in volts (a), current in amps (b). Stator winding is one turn of 20 AWG, H = 4 in., W = 1 in., R_s = 12.7 mΩ, L_s = 0.55 μH, with no series inductor: R_c = 0, L_c = 0.

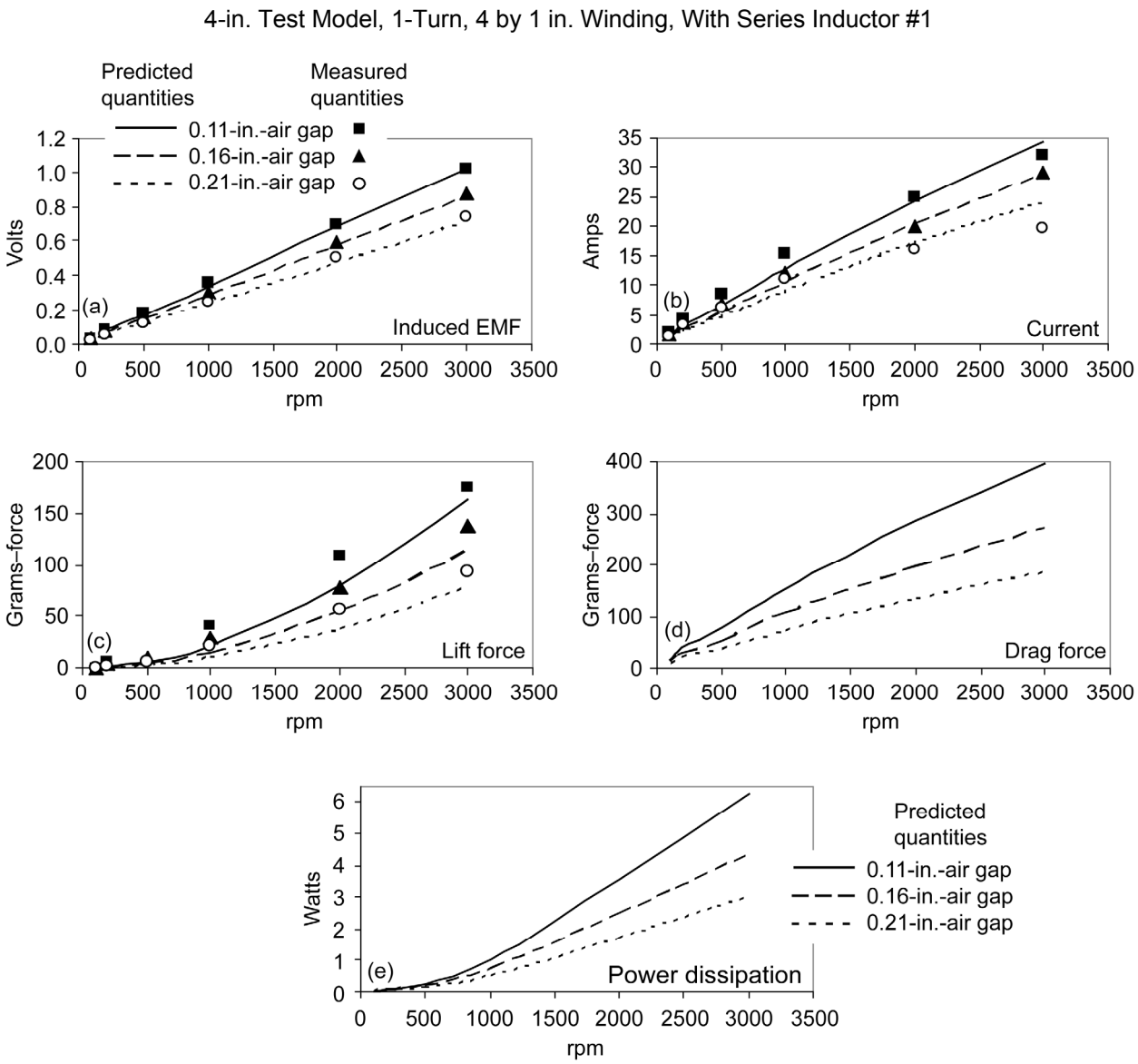

Figure A–8.—Plots of analytically predicted and measured quantities versus rpm for 4-in.-radial test model stator winding, including induced EMF in volts (a), current in amps (b), and lift force in grams–force (c). Predicted values only for drag force in grams–force (d) and power dissipation in watts (e).Stator winding is one turn of 20 AWG, H = 4 in., W = 1 in., R_S = 12.7 mΩ, L_S = 0.55 μH, with series inductor 1: R_C = 13.8 mΩ, L_C = 4.8 μH.

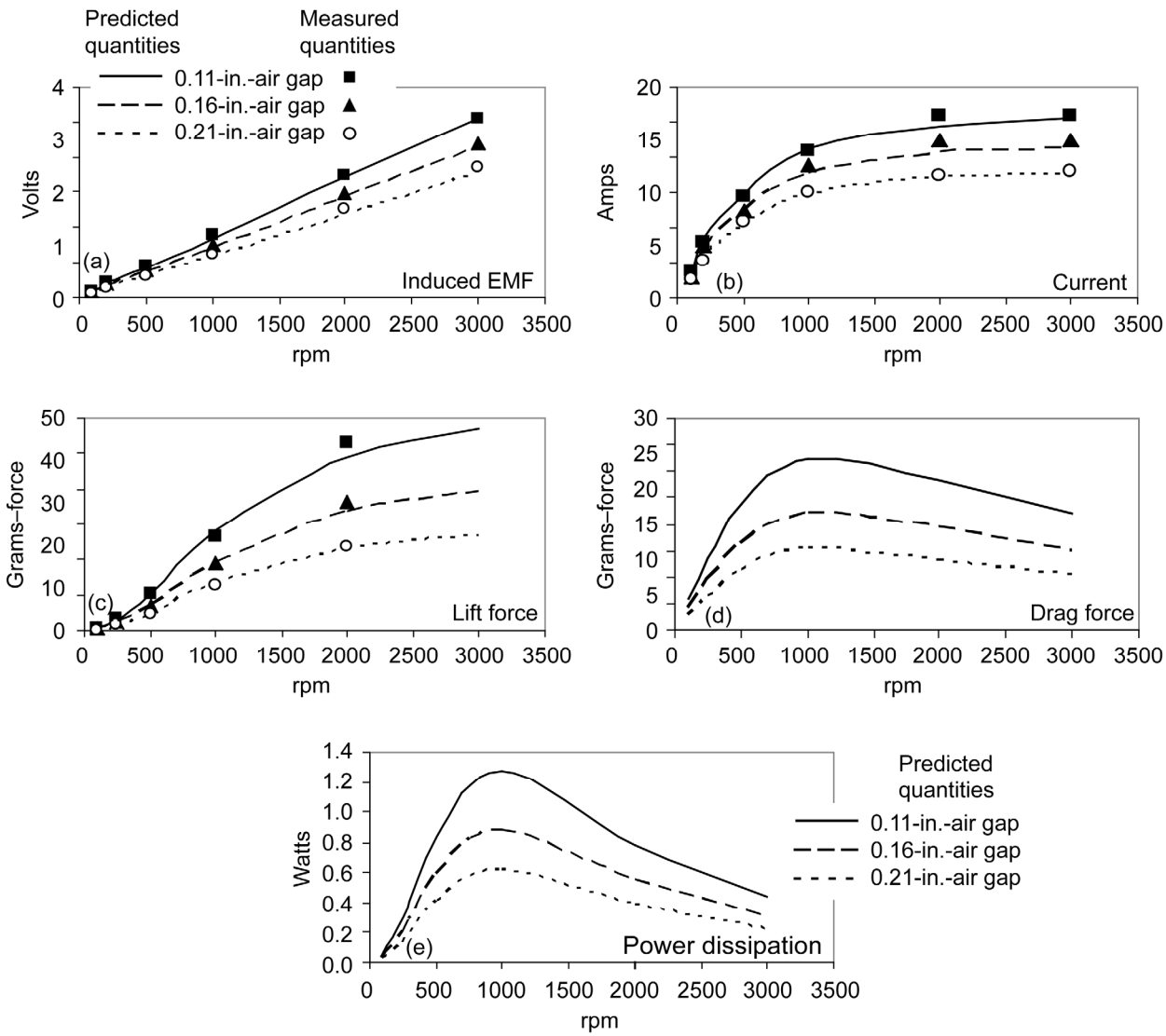

Figure A–9.—Plots of analytically predicted and measured quantities versus rpm for 4-in.-radial test model stator winding, including induced EMF in volts (a), current in amps (b), and lift force in grams–force (c). Predicted values only for drag force in grams–force (d) and power dissipation in watts (e).Stator winding is one turn of 20 AWG, H = 4 in., W = 1 in., R_S = 12.7 mΩ, L_S = 0.55 μH, with series inductor 2: R_C = 34.6 mΩ, L_C = 77.4 μH.

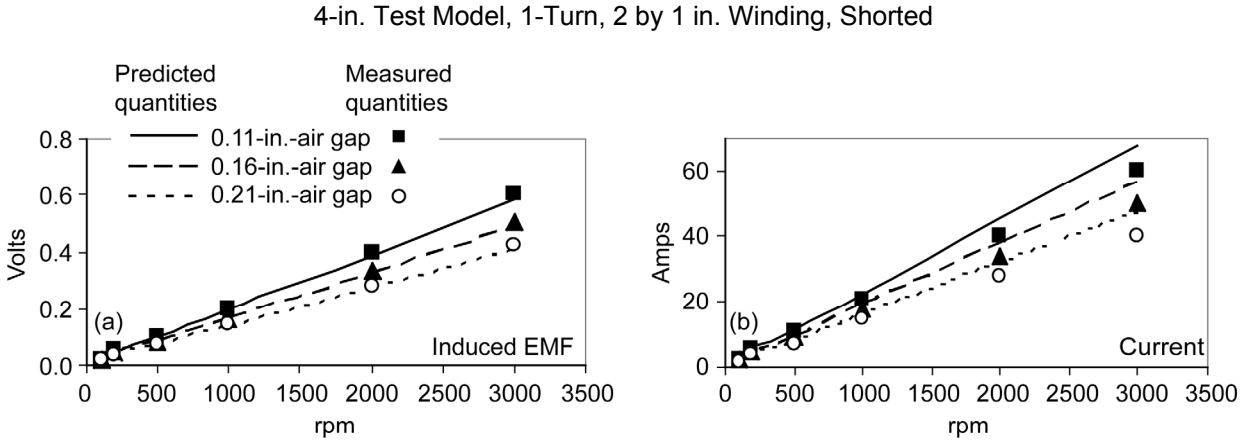

Figure A–10.—Plots of analytically predicted versus measured quantities versus rpm for 2-in.-radial test model stator winding, including induced EMF in volts (a), current in amps (b). Stator winding is one turn of 20 AWG, H = 4 in., W = 1 in., R_S = 8.6 mΩ, L_S = 0.38 μH, with no series inductor: R_C = 0, L_C = 0.

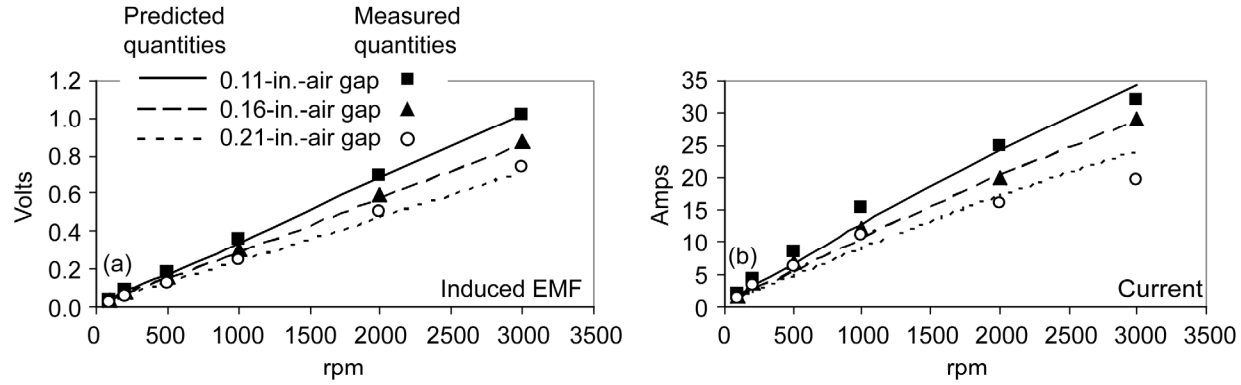

Figure A–11.—Plots of analytically predicted versus measured quantities for 4-in.-radial test model stator winding, including induced EMF in volts (a), current in amps (b). Stator winding is one turn of 20 AWG, H = 4 in., W = 1 in., R_S = 8.6 mΩ, L_S = 0.38 μH, with series inductor 1: R_C = 13.8 mΩ, L_C = 4.8 μH.

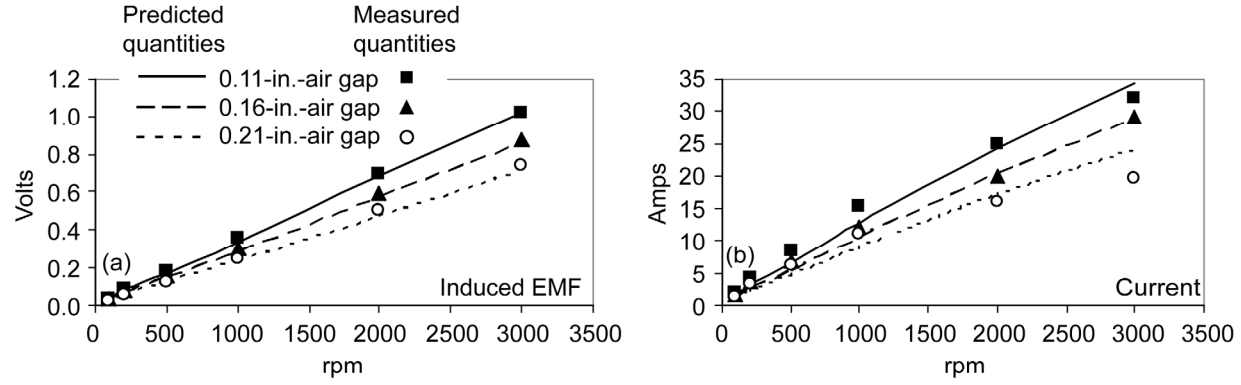

Figure A–12.—Plots of analytically predicted versus measured quantities for 4-in.-radial test model stator winding, including induced EMF in volts (a), current in amps (b). Stator winding is one turn of 20 AWG, H = 2 in., W = 1 in., R_S = 8.6 mΩ, L_S = 0.38 μH, with series inductor 2: R_C = 34.6 mΩ, L_C = 77.4 μH.

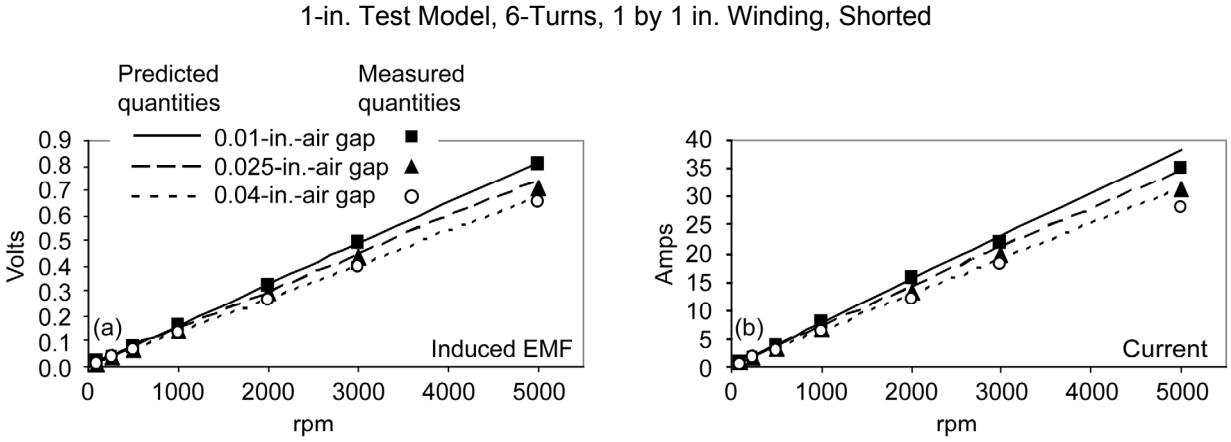

Figure A–13.—Plots of analytically predicted versus measured quantities for 1-in.-radial test model stator winding, including induced EMF in volts (a), current in amps (b). Stator winding is six turns of 20 AWG, H = 1 in., W = 1 in., R_s = 21 mΩ, L_s = 1.75 μH, with no series inductor: R_c = 0, L_c = 0.

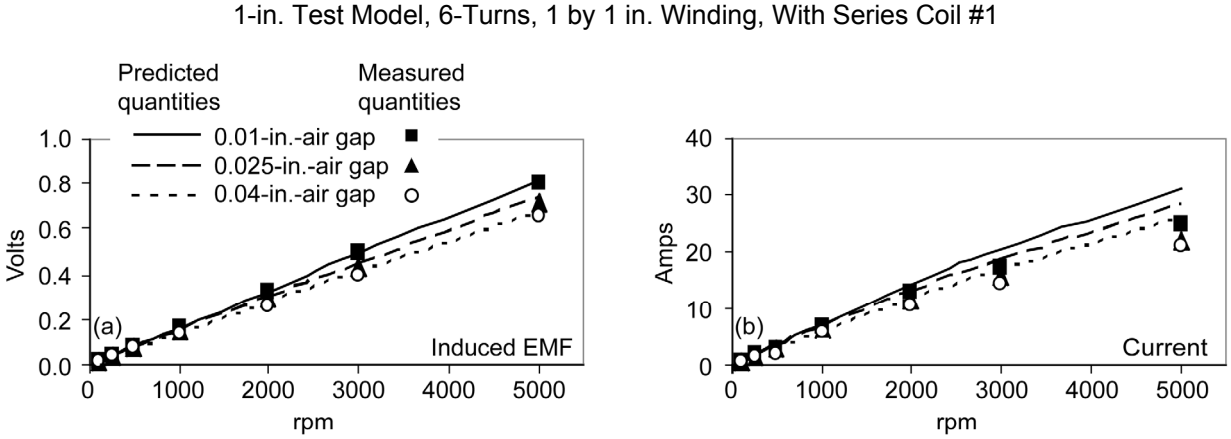

Figure A–14.—Plots of analytically predicted versus measured quantities for 1-in.-radial test model stator winding, including induced EMF in volts (a), current in amps (b). Stator winding is six turns of 20 AWG, H = 1 in., W = 1 in., R_s = 21 mΩ, L_s = 1.75 μH, with series inductor 1: R_c = 13.8 mΩ, L_c = 4.8 μH.

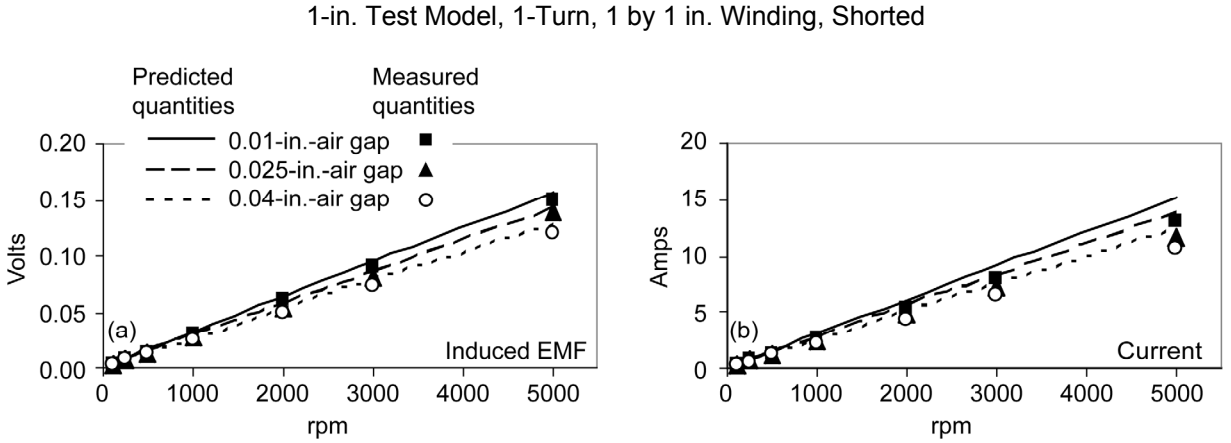

Figure A–15.—Plots of analytically predicted versus measured quantities for 1-in.-radial test model stator winding, including induced EMF in volts (a), current in amps (b). Stator winding is one turn of 20 AWG, H = 1 in., W = 1 in., R_s = 10.3 mΩ, L_s = 17 μH, with no series inductor: R_c = 0, L_c = 0.

REPORT DOCUMENTATION PAGE

Form Approved
OMB No. 0704-0188

1. AGENCY USE ONLY (*Leave blank*)	2. REPORT DATE	3. REPORT TYPE AND DATES COVERED
	December 2006	Technical Memorandum

4. TITLE AND SUBTITLE

Development and Testing of a Radial Halbach Magnetic Bearing

5. FUNDING NUMBERS

WBS 561581.02.08.03.06.04

6. AUTHOR(S)

Dennis J. Eichenberg, Christopher A. Gallo, and William K. Thompson

7. PERFORMING ORGANIZATION NAME(S) AND ADDRESS(ES)

National Aeronautics and Space Administration
John H. Glenn Research Center at Lewis Field
Cleveland, Ohio 44135–3191

8. PERFORMING ORGANIZATION REPORT NUMBER

E–15769

9. SPONSORING/MONITORING AGENCY NAME(S) AND ADDRESS(ES)

National Aeronautics and Space Administration
Washington, DC 20546–0001

10. SPONSORING/MONITORING AGENCY REPORT NUMBER

NASA TM—2006-214477

11. SUPPLEMENTARY NOTES

Responsible person, Dennis J. Eichenberg, organization code DEE, 216–433–8360.

12a. DISTRIBUTION/AVAILABILITY STATEMENT

Unclassified - Unlimited
Subject Category: 07

Available electronically at http://gltrs.grc.nasa.gov

This publication is available from the NASA Center for AeroSpace Information, 301–621–0390.

12b. DISTRIBUTION CODE

13. ABSTRACT ***(Maximum 200 words)***

The NASA John H. Glenn Research Center has developed and tested a revolutionary Radial Halbach Magnetic Bearing. The objective of this work is to develop a viable non-contact magnetic bearing utilizing Halbach arrays for all-electric flight, and many other applications. This concept will help reduce harmful emissions, reduce the Nation's dependence on fossil fuels and mitigate many of the concerns and limitations encountered in conventional axial bearings such as bearing wear, leaks, seals and friction loss. The Radial Halbach Magnetic Bearing is inherently stable and requires no active feedback control system or superconductivity as required in many magnetic bearing designs. The Radial Halbach Magnetic Bearing is useful for very high speed applications including turbines, instrumentation, medical applications, manufacturing equipment, and space power systems such as flywheels. Magnetic fields suspend and support a rotor assembly within a stator. Advanced technologies developed for particle accelerators, and currently under development for maglev trains and rocket launchers, served as the basis for this application. Experimental hardware was successfully designed and developed to validate the basic principles and analyses. The report concludes that the implementation of Radial Halbach Magnetic Bearings can provide significant improvements in rotational system performance and reliability.

14. SUBJECT TERMS

Magnetic bearings

15. NUMBER OF PAGES

39

16. PRICE CODE

17. SECURITY CLASSIFICATION OF REPORT	18. SECURITY CLASSIFICATION OF THIS PAGE	19. SECURITY CLASSIFICATION OF ABSTRACT	20. LIMITATION OF ABSTRACT
Unclassified	Unclassified	Unclassified	